



The Membrane Activity of the Amphibian Temporin B Peptide Analog TB_KKG6K Sheds Light on the Mechanism That Kills *Candida albicans*

Anant Kakar,^a Luis Enrique Sastré-Velásquez,^a Michael Hess,^b László Galgóczy,^{c,d} Csaba Papp,^e Jeanett Holzknicht,^a Alessandra Romanelli,^f Györgyi Váradi,^g  Nermina Malanovic,^h  Florentine Marx^a

^aBiocenter, Institute of Molecular Biology, Medical University of Innsbruck, Innsbruck, Austria

^bInstitute for Histology and Embryology, Medical University of Innsbruck, Innsbruck, Austria

^cDepartment of Biotechnology, Faculty of Science and Informatics, University of Szeged, Szeged, Hungary

^dInstitute of Biochemistry, Biological Research Centre, Eötvös Loránd Research Network, Szeged, Hungary

^eDepartment of Microbiology, Faculty of Science and Informatics, University of Szeged, Szeged, Hungary

^fDepartment of Pharmaceutical Sciences, University of Milan, Milan, Italy

^gDepartment of Medical Chemistry, Albert Szent-Györgyi Medical School, University of Szeged, Szeged, Hungary

^hInstitute of Molecular Biosciences, Field of Excellence BioHealth, University of Graz, Graz, Austria

ABSTRACT Temporin B (TB) is a 13-amino-acid-long, cationic peptide secreted by the granular glands of the European frog *Rana temporaria*. We recently showed that the modified TB peptide analog TB_KKG6K rapidly killed planktonic and sessile *Candida albicans* at low micromolar concentrations and was neither hemolytic nor cytotoxic to mammalian cells *in vitro*. The present study aimed to shed light into its mechanism of action, with a focus on its fungal cell membrane activity. We utilized different fluorescent dyes to prove that it rapidly induces membrane depolarization and permeabilization. Studies on model membrane systems revealed that the TB analog undergoes hydrophobic and electrostatic membrane interactions, showing a preference for anionic lipids, and identified phosphatidylinositol and cardiolipin as possible peptide targets. Fluorescence microscopy using fluorescein isothiocyanate-labeled TB_KKG6K in the presence of the lipophilic dye FM4-64 indicated that the peptide compromises membrane integrity and rapidly enters *C. albicans* cells in an energy-independent manner. Peptide-treated cells analyzed by cryo-based electron microscopy exhibited no signs of cell lysis; however, subcellular structures had disintegrated, suggesting that intracellular activity may form part of the killing mechanism of the peptide. Taken together, this study proved that TB_KKG6K compromises *C. albicans* membrane function, which explains the previously observed rapid, fungicidal mode of action and supports its great potential as a future anti-*Candida* therapeutic.

IMPORTANCE Fungal infections with the opportunistic human pathogen *C. albicans* are associated with high mortality rates in immunocompromised patients. This is partly due to the yeast's ability to rapidly develop resistance toward currently available antifungals. Small, cationic, membrane-active peptides are promising compounds to fight against resistance development, as many of them effectuate rapid fungal cell death. This fast killing is believed to hamper the development of resistance, as the fungi do not have sufficient time to adapt to the antifungal compound. We previously reported that the synthetic variant of the amphibian TB peptide, TB_KKG6K, rapidly kills *C. albicans*. In the current study, the mechanism of action of the TB analog was investigated. We show that this TB analog is membrane-active and impairs cell membrane function, highlighting its potential to be developed as an attractive alternative anti-*C. albicans* therapeutic that may hinder the development of resistance.

Editor Aaron P. Mitchell, University of Georgia

Copyright © 2022 Kakar et al. This is an open-access article distributed under the terms of the [Creative Commons Attribution 4.0 International license](https://creativecommons.org/licenses/by/4.0/).

Address correspondence to Florentine Marx, florentine.marx@i-med.ac.at, or Nermina Malanovic, nermina.malanovic@uni-graz.at.

The authors declare no conflict of interest.

Received 16 June 2022

Accepted 27 July 2022

Published 16 August 2022

KEYWORDS Temporin B, TB analog, antifungal peptide, *Candida albicans*, membrane activity, depolarization, permeabilization, leakage, uptake

Fungal infections (mycoses) range from superficial infections, e.g., of the skin, nails, and mucous membranes, to systemic infections that enmesh a number of organs, such as the brain, heart, lungs, liver, spleen, and kidneys. While the former category of fungal infections is not fatal and relatively straightforward to treat, the latter can be life-threatening, especially for immunocompromised patients, whose number is increasing due to heightened immunosuppressant usage, necessitated by the magnitude of transplant recipients and patients undergoing chemotherapy (1, 2). Currently, 150 million severe cases of mycoses occur worldwide each year, resulting in around 1.7 million deaths (3). The opportunistic human yeast pathogen *Candida albicans* is responsible for about 70% of fungal infections globally, making it the most common causative agent of mycoses in humans. Alarmingly, it is associated with mortality rates of over 40%, even with antifungal intervention (4).

The currently available antifungal drug repertoire is limited, and this dismal scenario is aggravated by the rise of resistance in fungi toward the major drug classes used as first-line therapy (5).

Antimicrobial peptides (AMPs) are currently the subject of extensive investigation as promising alternative therapeutic modalities against microbial infections. AMPs, the majority of which are small, cationic peptides that are essential components of the innate immune response of many organisms, are effective against a variety of human pathogenic fungi (5, 6).

Temporins are secreted by the granular glands of the European red frog *Rana temporaria* and form one of the largest families of amphibian AMPs. They are short (8 to 14 amino acids), mildly cationic (0 to +3 at pH 7), and hydrophobic (~50% hydrophobic amino acids) peptides that are predominantly active against Gram-positive bacteria (7, 8). Recently, several modifications were made to the primary structure of the membrane-active peptide Temporin B (TB) in order to increase its efficacy and broaden its antimicrobial spectrum (9–11). The peptide analog that resulted in the highest growth-inhibitory activity against both Gram-positive and Gram-negative bacteria was TB_KKG6K (TB analog; amino acid sequence KKLLPIVKNLLKSLI; molecular weight [MW], 1,718.2 Da); TB_KKG6K contains four lysine residues, of which two were added to the N terminus and one replaced the glycine (position 6) of the parent peptide. The new TB analog exhibits an increased positive net charge (from +0.9 to +3.9 at pH 7) and reduced hydrophobicity (from 61% to 53% hydrophobic amino acids), as well as a modified amphipathic profile (10). Previous studies on synthetic TB_KKG6K were primarily focused on its antibacterial activity (10); however, its antifungal potential was less thoroughly investigated. We therefore recently evaluated its efficacy against the opportunistic human pathogen *C. albicans* (7). We demonstrated that the peptide acted in a rapid and fungicidal manner against planktonic and sessile *C. albicans* cells, facilitating efficacious cell killing at low micromolar concentrations. In addition, we were able to demonstrate that this peptide is well tolerated by primary human skin cells and three-dimensional skin epidermal models *in vitro*, indicating its potential as a therapeutic alternative against *C. albicans* skin infections (7).

The TB analog's established antifungal efficacy encouraged us to further investigate this peptide in the current study by shifting our attention to its mechanism of action. We chose to focus on its activity on the fungal cell membrane because of the compound's small size, positive charge, and rapid fungicidal mode of action (7), which are characteristic features of cell membrane-active AMPs (12, 13). A multidisciplinary approach revealed that the TB analog compromised membrane function and rapidly entered the *C. albicans* cells, where it disintegrated subcellular structures. The obtained results prove that this peptide is a promising, membrane-active amphibian biomolecule with the potential to join the next generation of peptide anti-*Candida* therapeutics.

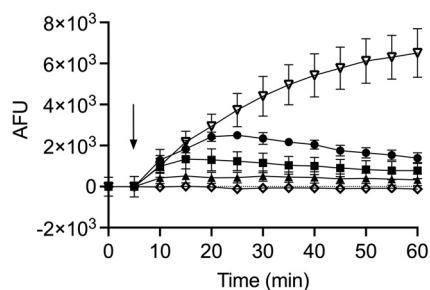


FIG 1 Membrane depolarization potential of TB_KKG6K in *C. albicans*, determined with DiSC₃(5) dye. Filled symbols show results for TB peptide at 0.5 μM (\blacktriangle), 1 μM (\blacksquare), and 2 μM (\bullet); open symbols show results with the controls Triton X-100 at 1% (wt/vol) (∇) and PC $\gamma^{\text{C-terminal}}$ at 32 μM (\diamond). Compound addition is marked with an arrow, and the depolarization of the cell membrane was monitored over a 60-min time period. The arbitrary fluorescence units (AFU) shown have been normalized by subtracting the background fluorescence values of the *C. albicans*-DiSC₃(5) combination without compound addition (untreated control). The values represent the means \pm standard deviation (SD) of fluorescence values collected from two independent experiments performed in technical duplicates.

RESULTS

Determination of growth-inhibitory concentrations of test compounds. The inhibitory concentration that reduced the growth of *C. albicans* (CBS 5982) by $\geq 90\%$ (IC_{90}) was determined for TB_KKG6K, *N,N'*-(1,10 decanediyldi-1[4H]-pyridinyl-4-ylidene)-bis-(1-octanamine) dihydrochloride (octenidine, the positive control), and PC $\gamma^{\text{C-terminal}}$ (negative control) in broth microdilution assays using two yeast cell concentrations (1×10^4 and 1×10^6 cells/mL), as some experiments required different cell numbers. TB_KKG6K had an IC_{90} of 2 μM irrespective of the cell concentration used. This value corresponded to the previously reported IC_{90} determined against *C. albicans* by our group (7). Octenidine yielded an IC_{90} of 1 μM with 1×10^4 cells/mL and 2 μM with 1×10^6 cells/mL. As described previously (14), the peptide PC $\gamma^{\text{C-terminal}}$ (amino acid sequence CGGASCRG; MW 709.8 Da), which is derived from the C-terminal part of the *Penicillium chrysogenum* anti-fungal protein C (PAFC), was found to be inactive against *C. albicans*. No fungal growth inhibition at the administered peptide concentration (0 to 32 μM) was detected.

TB_KKG6K impairs the cell membrane integrity of *C. albicans*. To investigate how TB_KKG6K affects the integrity of the cell membrane of *C. albicans*, we first tested if the TB analog disrupted membrane polarity. To this end, we used the voltage-sensitive fluorescent dye 3,3'-dipropylthiadicarbocyanine iodide [DiSC₃(5)], which dimerizes and accumulates in the intact polarized cell membrane of energized cells, resulting in quenching of the fluorescent signal. Upon membrane depolarization, the DiSC₃(5) dimers dissociate and are released into the supernatant. The release can be measured as an increase in fluorescence intensity (15). The membrane-perturbing surfactant Triton X-100 was used as a positive control at a concentration of 1% (wt/vol). It induced a fast and sustained increase in fluorescence intensity, proving that it dissipated the cell membrane potential in a timely manner (Fig. 1). PC $\gamma^{\text{C-terminal}}$ was applied at 32 μM and served as the negative control. No membrane depolarization was observed with PC $\gamma^{\text{C-terminal}}$ (Fig. 1). The TB analog was applied in three different concentrations, 0.5 μM , 1 μM , and 2 μM . TB_KKG6K induced membrane depolarization in a concentration- and time-dependent manner. The fluorescence intensity of the sample immediately increased upon the addition of 2 μM peptide (corresponding to the IC_{90} value) within the first 25 min of exposure. The response was less pronounced when the peptide was added at the subinhibitory concentration of 1 μM and minimal with 0.5 μM (Fig. 1). This result indicated that TB_KKG6K dissipates the cell membrane potential, which might be one reason for its growth-inhibitory activity against *C. albicans*.

Next, we questioned whether the depolarization of the cell membrane by the TB analog coincided with its permeabilization. We therefore tested the membrane-permeabilizing capacity of TB_KKG6K with the SYTOX green uptake assay. The fluorescent SYTOX green dye is a membrane-impermeable molecule that penetrates only compromised cell

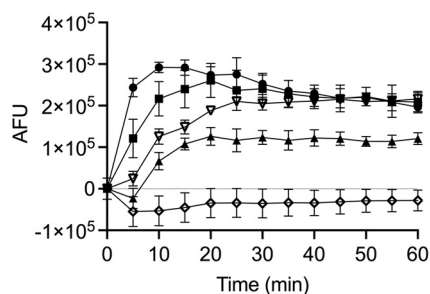


FIG 2 Membrane permeabilization activity of TB_KKG6K in *C. albicans* detected with the SYTOX green uptake assay. Filled symbols show results with TB peptide at 0.5 μM (\blacktriangle), 1 μM (\blacksquare), or 2 μM (\bullet); open symbols show results for the controls, octenidine at 2 μM (∇) or $\text{PC}\gamma\text{C-terminal}$ at 32 μM (\diamond). AFU were normalized by subtracting the background fluorescence of the medium with or without compounds in the absence of cells. AFU values depicted in the graph were further corrected by subtracting the fluorescence values of the *C. albicans*-SYTOX green combination without compound addition (untreated control). The values presented are the means \pm SD determined from two independent experiments performed in technical duplicates.

membranes and fluoresces upon binding to nucleic acids (16). This was confirmed by the use of the positive control octenidine, which is a membrane-active compound previously shown to possess anti-*Candida* activity (17). Octenidine increased the fluorescence intensity of the sample after its addition at its IC_{90} (2 μM) (Fig. 2). TB_KKG6K was applied at 0.5 μM , 1 μM , and 2 μM , and the change in fluorescence intensity after peptide addition was monitored for 60 min (Fig. 2). Within the first 10 min of incubation, the rise in fluorescence intensity induced with 2 μM peptide was the fastest, followed by that of the sample exposed to 1 μM peptide. Steady-state signal intensity values were reached after 15 to 20 min of incubation with both peptide concentrations, which settled thereafter at a level similar to that of the positive control octenidine. The permeabilization of the membrane was delayed and less effective when 0.5 μM peptide was used. The negative control $\text{PC}\gamma\text{C-terminal}$ showed no membrane-permeabilizing activity (Fig. 2). Of note, the negative fluorescence values recorded with $\text{PC}\gamma\text{C-terminal}$ might be explained by the peptides' possible interference with SYTOX green, thereby preventing the interaction of the dye with the cell. The fact that the exposure of cells to TB_KKG6K resulted in a fast depolarization and permeabilization of the cell membrane indicates that the TB analog quickly kills *C. albicans* by compromising cell membrane integrity.

TB_KKG6K binds to phosphoinositide phosphates and preferentially permeabilizes anionic model membranes. Many cationic effector peptides of natural and synthetic origin have been reported to be specifically attracted by negatively charged membrane components, e.g., phospholipids, and these interactions have been shown to regulate their mode of antimicrobial action (18). We therefore tested, in a proof-of-principle experiment, the cationic TB analog for its ability to bind to the lipid head groups via electrostatic interactions. To this effect, we performed a peptide-lipid overlay experiment using commercially available phosphatidylinositol phosphate (PIP) strips. Since antibodies directed against TB_KKG6K were not available, we used the peptide labeled with the green fluorophore fluorescein isothiocyanate (FITC; FITC-TB_KKG6K) and recorded the fluorescence intensity of the signal of the lipid-bound peptide on the membrane. As shown in Fig. 3A, the peptide exhibited a preferential binding to lipids with a higher negative charge, namely, phosphatidylinositol (PI) mono-, bi-, and triphosphates. Semiquantification of the spot signal intensity on the membranes ($n = 3$) confirmed the preference of TB_KKG6K for phosphorylated PI, but also for unphosphorylated PI (Fig. 3B). The binding to phosphatidic acid (PA) and phosphatidylserine (PS), however, was not significantly higher than that with the blank (Fig. 3B). No binding of the peptide occurred with lysophosphatidic acid (LPA), lysophosphocholine (LPC), phosphatidylethanolamine (PE), phosphatidylcholine (PC), or sphingosine-1-phosphate (S1P) (Fig. 3A and B).

To gain more detailed insights into the binding preferences of TB_KKG6K for certain lipids that influence its interaction with the cell membrane, we evaluated the peptide's

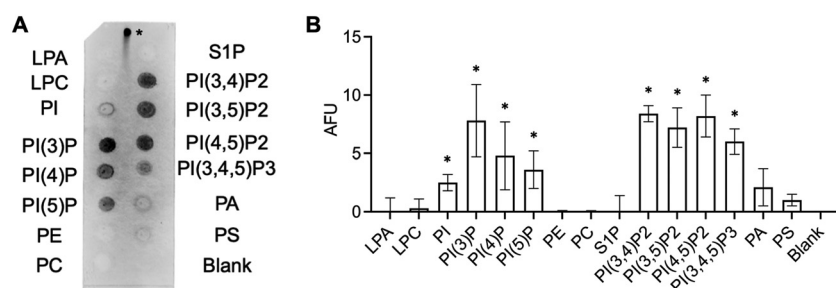


FIG 3 Binding of FITC-TB_KKG6K to phosphoinositide phosphates. (A) The PIP strip was probed with 1.5 $\mu\text{g}/\text{mL}$ of FITC-labeled TB_KKG6K, and binding of the peptide to the lipids was fluorometrically detected. The positive control for fluorescence signal detection is marked with an asterisk and represents 0.5 μg of peptide spotted onto the membrane. The PIP strip shown represents the result of one out of three independent experiments. (B) Relative quantification of signal intensities of the spots representing TB_KKG6K bound to lipids, compared to the blank, which was set as 0 AFU. AFU represent the means \pm SD of fluorescence values quantified in three independent blots by ImageJ/FIJI. *, $P \leq 0.05$. LPA, lysophosphatidic acid; LPC, lysophosphocholine; PIP, phosphoinositide phosphates; PE, phosphatidylethanolamine; PC, phosphatidylcholine; S1P, sphingosine-1-phosphate; PA, phosphatidic acid; PS, phosphatidylserine.

permeabilizing potential by using large unilamellar vesicles (LUVs) of different lipid composition and charge that represented prokaryotic and eukaryotic model membranes. The LUVs were loaded with 8-aminonaphthalene-1,3,6-trisulfonic acid and *p*-xylene-bispyridinium bromide (ANTS-DPX) which, upon the application of a permeabilizing compound, leaks out into the surrounding buffer and can be quantified fluorometrically (19–21). These changes in fluorescence intensity were followed in real time before and 30 min after the addition of the compounds to be examined. The negative and positive controls used in this experiment were 32 μM $\text{PC}\gamma^{\text{C-terminal}}$ and the membrane-lysing surfactant agent Triton X-100 (1% [wt/vol]), respectively. The fluorescence intensity values that were reached due to the leakage of ANTS-DPX of LUVs exposed to the positive control represented 100% leakage. No membrane activity ($\leq 2\%$ leakage) was induced in LUVs by the negative control, $\text{PC}\gamma^{\text{C-terminal}}$ (Table 1). The peptide was applied in three concentrations, 2 μM , 4 μM , and 8 μM (representing lipid-to-peptide molar ratios of 25:1, 12:1, and 6:1, respectively) (Table 1).

Due to the well-characterized cell membrane activity of TB on bacteria, we first performed a control experiment and tested two model membranes that were composed of the main constituents of bacterial membranes, the anionic phosphatidylglycerol (PG), cardiolipin (CL), and the zwitterionic PE (22–25). The LUVs contained either PG alone (100% anionic), mimicking the membrane of Gram-positive bacteria, or a mixture of PG, PE, and CL (PE-PG-CL, 30% anionic), representing the membrane of Gram-negative bacteria. As expected, TB_KKG6K interacted with both model membranes (Table 1). The leakage of LUVs composed of the less-anionic lipids PE-PG-CL was strongly concentration dependent, whereby 8 μM peptide was required to reach $61\% \pm 3\%$ membrane leakage (mean \pm standard deviation [SD]). In contrast, model membranes consisting of only PG were affected at a much lower peptide concentration; the exposure to 2 μM peptide resulted in $56\% \pm 4\%$ leakage, a value that increased only slightly with 8 μM peptide ($61\% \pm 4\%$). This indicated that the maximum possible peptide-induced leakage of LUVs was reached in this experimental setting and pointed toward the peptide's preference for anionic membranes (Table 1).

Next, we wanted to evaluate whether the TB analog prefers anionic membranes over neutral ones. Therefore, we compared the leakage elicited in LUVs composed of anionic PG to those containing the neutral PC. As shown in Table 1, TB_KKG6K interacted with PC and induced leakage in a concentration-dependent manner; however, the leakage values induced at all peptide concentrations tested were significantly higher ($P \leq 0.05$) with PG than with PC (differences in leakage with PG compared with PC: +40% at 2 μM , +30% at 4 μM , +20% at 8 μM). Although the peptide favored interaction with the anionic PG, the fact that it induced leakage in the zwitterionic PC

TABLE 1 TB_KKG6K-induced leakage of microbial model membranes^a

Model	Lipid(s) and location	% Leakage			PC γ ^{C-terminal} (32 μ M)
		TB_KKG6K			
		2 μ M	4 μ M	8 μ M	
Prokaryotic membrane	PG	56.0 \pm 4.0* (+40)	57.7 \pm 3.9* (+30)	61.1 \pm 4.1* (+20)	1.9 \pm 1
	PG-PE-CL	5.3 \pm 1.3	40.2 \pm 0.9	61.5 \pm 2.7	-1.2 \pm 1.6
Eukaryotic membrane	PC	33.8 \pm 3.0	40.6 \pm 3.2	49.2 \pm 4.5	1.4 \pm 1.4
	Outer leaflet				
	PC-sphingomyelin	18.8 \pm 3.1* (-44)	26.5 \pm 1.0* (-34)	33.9 \pm 2.0* (-31)	0.6 \pm 0.8
	PC-ceramide	17.9 \pm 1.8* (-47)	39.9 \pm 2.4	44.8 \pm 1.9	1.3 \pm 0.2
	Inner leaflet				
	PC-PI	37.7 \pm 3.9	52.5 \pm 2.4* (+29)	56.5 \pm 2.9* (+15)	0.4 \pm 0.5
	PC-PE	22.8 \pm 1.3* (-32)	31.5 \pm 2.1* (-22)	40.0 \pm 3.1* (-19)	1.4 \pm 0.6
	PC-PS	22.6 \pm 3.3* (-33)	38.1 \pm 10.5	47.4 \pm 15.1	0.9 \pm 2.7
	PC-ergosterol	9.8 \pm 1.5* (-71)	13.0 \pm 0.6* (-68)	16.9 \pm 2.0* (-66)	1.1 \pm 0.9
	PC-PE-ergosterol	14.8 \pm 0.8* (-56)	17.1 \pm 6.0* (-58)	15.8 \pm 1.3* (-68)	1.7 \pm 2.0
	PC-PS-ergosterol	21.8 \pm 3.5* (-36)	30.1 \pm 4.6* (-26)	46.3 \pm 4.2	2.0 \pm 1.4
	Mitochondrial envelope				
	PC-CL	2.2 \pm 0.8* (-93)	9.9 \pm 0.7* (-75)	59.0 \pm 5.8* (+20)	0.7 \pm 0.4

^aData represent leakage of 50 μ M concentrations of model membranes composed of different lipids in response to exposure to 2 μ M, 4 μ M, or 8 μ M TB_KKG6K, which corresponded to lipid:peptide molar ratios of 25:1, 12:1, and 6:1, respectively, determined after 30 min of incubation at 37°C. Data are relative mean \pm SD leakage of two independent experiments performed in duplicates in the presence of the TB analog. The values were compared to those for the positive control (1% [wt/vol] Triton-X), which represented 100% leakage. The relative change (as a percentage) in leakage of the different lipid combinations was compared to the values for PC-LUVs (in parentheses). PC γ ^{C-terminal} (32 μ M; lipid:peptide molar ratio of 1.5:1) served as a negative control. A two-way ANOVA, corrected for multiple comparisons by the Dunnett's test, was applied to calculate the significant differences between the mean leakage values of LUVs composed of distinct lipid formulations to those of the PC-LUVs. *, $P \leq 0.05$.

as well suggests that not only electrostatic but also other forces, such as hydrophobic or hydrogen bonding, are involved in the interaction with the cell membrane lipids.

Finally, we tackled the question of whether the TB peptide preferentially targets membranes containing any specific lipid. To this end, we performed leakage studies using nine eukaryotic model membranes composed of PC along with one or two more lipids specific to eukaryotic membranes, namely, CL, ceramide, ergosterol, PE, PI, PS, and sphingomyelin. PC formed the dominant part of these LUVs, as this neutral phospholipid is a major component of fungal and mammalian cell membranes (26, 27).

The leakage measurements revealed that among all the tested eukaryotic membrane formulations, the sensitivity of LUVs toward 2 μ M and 4 μ M TB_KKG6K was higher than that with PC alone only when this neutral lipid was combined with PI (increase in leakage compared to PC alone: +29% at 4 μ M, +15% at 8 μ M). The leakage of LUVs containing PC-CL was also higher (+20%) than that of PC alone in the presence of 8 μ M peptide. Membranes composed of PC and ceramide, PE, or PS did not yield higher leakage values compared to levels observed with PC-LUVs (Table 1). This let us assume that these lipids neither represent potential targets of TB_KKG6K nor increase membrane susceptibility for the peptide.

Of note, the presence of ergosterol or sphingomyelin in PC hampered the membrane activity of TB_KKG6K and inhibited the leakage of ANTS-DPX from LUVs composed of PC-sphingomyelin and PC-ergosterol, respectively (Table 1). The addition of ergosterol to zwitterionic PC-PE or charged PC-PS similarly inhibited the leakage of PC-PE-ergosterol or PC-PS-ergosterol, but not of PC-PS-ergosterol when exposed to the highest peptide concentration applied (8 μ M), suggesting that the anionic phospholipid PS can compensate for ergosterol's inhibitory effect on leakage induction (Table 1).

The physicochemical properties of TB_KKG6K favor membrane partitioning.

The Membrane Protein Explorer software mPEX v.3.3.0 was applied to investigate the membrane-partitioning properties of the TB_KKG6K *in silico*, using the AMP LL-37 (with residues 13 to 37 applied to compute parameters, i.e., LL-37₁₃₋₃₇) as a reference. This well-characterized AMP has previously been shown to be membrane-active and toxic to *C. albicans* (28). Fig 4 depicts the helical wheel projections of both peptides,

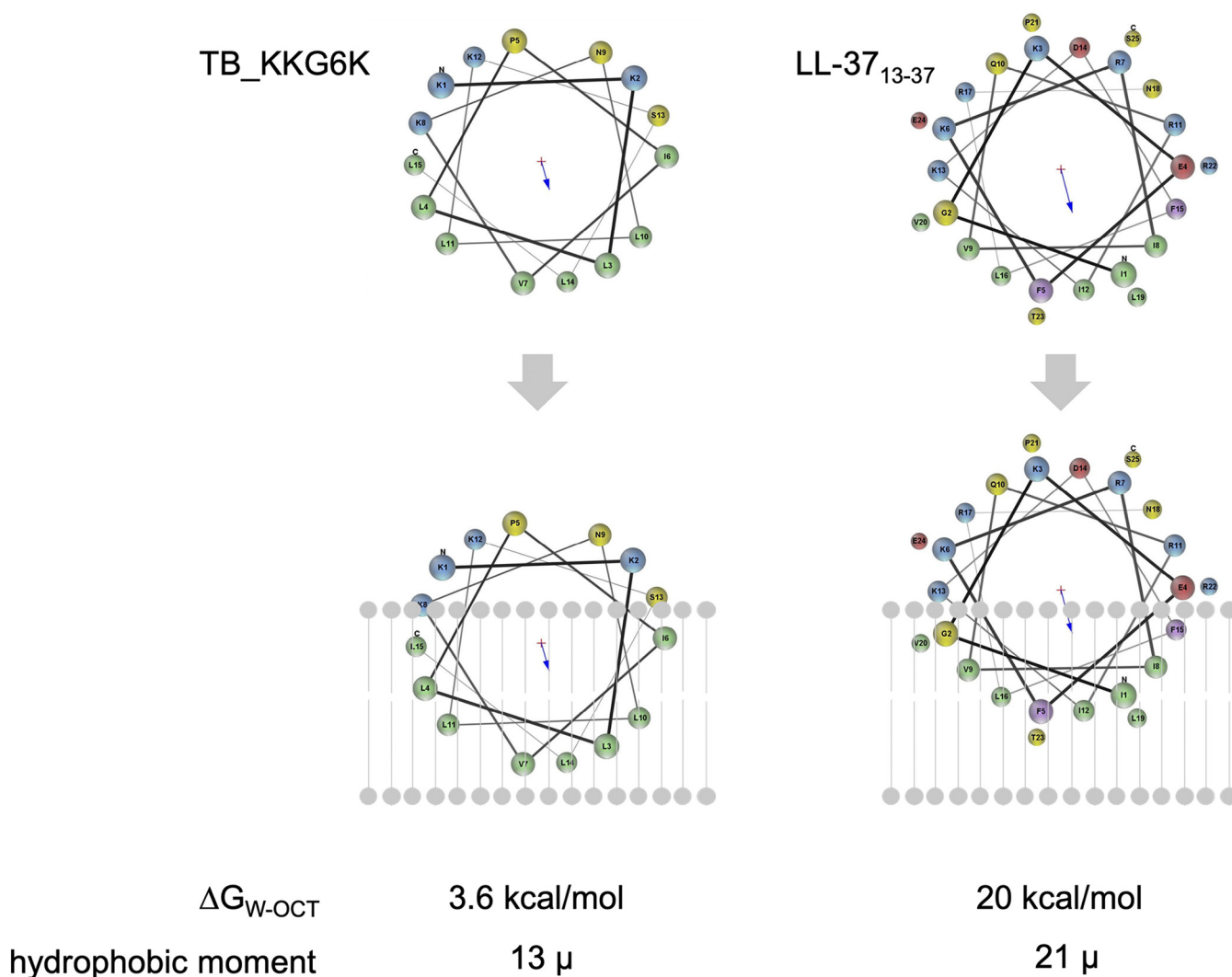


FIG 4 Results of *in silico* evaluation of peptide-membrane binding. (The helical wheel projections of TB_KKG6K and LL-37₁₃₋₃₇ [reference peptide] were performed with Membrane Protein Explorer mPEX [31]). The proposed partitioning of each peptide into the phospholipid bilayer (scheme in gray) is shown. The bilayer partitioning free energy (ΔG_{W-OCT}) is indicated in kilocalories per mole, and the hydrophobic moment (extent of amphipathicity) is indicated by μ for both peptides. Negatively charged residues are shown in red, positively charged are in blue, aliphatic are in green, polar are in yellow, and aromatic are in violet.

indicating that both possess localized hydrophobic regions that could facilitate their interaction with and insertion into the hydrophobic membrane bilayer. This hydrophobic region, however, is larger in the TB analog (53% hydrophobic amino acids), as it consists of eight uncharged, hydrophobic residues, in comparison to the five hydrophobic amino acids in LL-37₁₃₋₃₇ (40% hydrophobic amino acids), indicating that TB_KKG6K might be able to insert deeper into the membrane than LL-37₁₃₋₃₇. The TB analog, however, contains only four charged residues in its predicted α -helix, compared to six in LL-37₁₃₋₃₇, implying that TB_KKG6K can undergo electrostatic interactions with the negatively charged membrane, but that the membrane attraction is less pronounced than in the case of LL-37₁₃₋₃₇. According to the bilayer-partitioning free energy calculation, the TB analog required less energy to enter the bilayer (3.6 kcal/mol) than did LL-37₁₃₋₃₇ (20 kcal/mol) (Fig. 4). Calculation of the amphipathicity of the respective peptide α -helices revealed that the hydrophobic moment of the TB analog was lower (13 μ) than that of LL-37 (21 μ) (Fig. 4). This implies that the hydrophobic and hydrophilic residues are more evenly distributed among the helix of TB_KKG6K, resulting in increased amphipathicity, which in turn facilitates membrane binding and insertion (29–31).

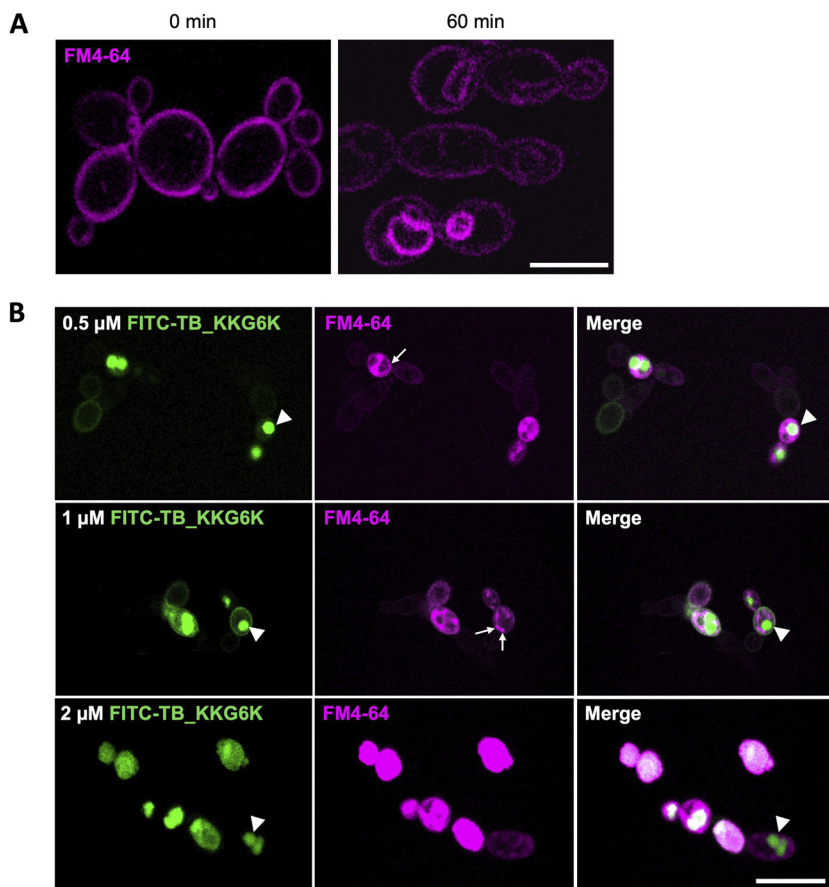


FIG 5 Laser scanning microscopic imaging of *C. albicans* stained with FM4-64 and treated with FITC-labeled TB_KKG6K in *C. albicans*. (A) The binding of 0.8 μM FM4-64 to the cell membrane and intracellular membranes was monitored in *C. albicans* incubated for 0 min and 60 min at 30°C. (B) Cells were exposed to 0.5 μM , 1 μM , and 2 μM peptide in the presence of 0.8 μM FM4-64 for 5 min at 30°C. Presumptive vacuoles and prevacuolar compartments are marked with arrowheads and small arrows, respectively. Scale bar, 5 μm (A) or 10 μm (B).

TB_KKG6K rapidly enters *C. albicans* cells. After identifying TB_KKG6K as a membrane-active peptide in *C. albicans*, we wanted to track its cellular localization and to assess whether it is retained in the cell membrane or enters the target cell. To this end, we used FITC-TB_KKG6K, which had been confirmed to have the same anti-*Candida* activity as the unlabeled peptide (data not shown). Before treatment with the FITC-labeled TB analog, *C. albicans* cells were stained with 0.8 μM *N*-(3-triethylammoniumpropyl)-4-(6-(4-(diethylamino) phenyl) hexatrienyl) pyridinium dibromide (FM4-64, a fluorescent styryl dye) to observe its membrane distribution by laser scanning microscopy (LSM) (Fig. 5). FM4-64 first interacted with the cell membrane, which appeared brightly stained. Over time, the signal faded from the cell membrane due to the dye's endocytic transport into the cells, where it stained intracellular membranes (Fig. 5A). We then assessed the localization of 0.5 μM , 1 μM , and 2 μM FITC-TB_KKG6K in the presence of FM4-64. Immediately after addition of the peptide at the subinhibitory concentrations of 0.5 μM or 1 μM to the cells, the peptide-specific FITC signal localized at the cell membrane and accumulated intracellularly in round compartments, presumably vacuoles. In some cells, however, the fluorescence appeared dispersed throughout the cytoplasm (Fig. 5B). The intensity of the cytoplasmic fluorescent signal dramatically increased when the cells were exposed to 2 μM FITC-TB_KKG6K, which corresponded to its IC_{50} (Fig. 5B). Furthermore, the number of peptide-containing cells increased in proportion to the applied peptide concentration, and at 2 μM the peptide had entered almost all of the cells in the focal plane (see Fig. S1 in the supplemental material). Of note, in the presence

of 0.5 μM or 1 μM peptide, FM4-64 fluorescence was not retained in the cellular membranes, as was the case in the control cells (Fig. 5A); rather, the dye accumulated in presumptive prevacuolar compartments or was found dispersed throughout the cytoplasm (Fig. 5B). With 2 μM FITC-TB_KKG6K treatment, the FM4-64 fluorescence signal had dissipated throughout the whole cell, where it colocalized with that of the peptide (Fig. 5B; see also Fig. S1). This observation suggested that the peptide's activity disturbed the membrane accumulation of FM4-64 and further underlined that TB_KKG6K affects the integrity of the cell membrane and the intracellular membranes. No retention of the peptide in the cell wall was observed (see Fig. S2A and B in the supplemental material).

The extremely fast interaction of the peptide with the *C. albicans* cells was further confirmed by fluorescence-activated cell sorting (FACS) analysis. The relative amount of FITC-positive cells was quantified after 5 min and 30 min of peptide exposure. After only 5 min of incubation, $89.7\% \pm 8.6\%$ of the 5,000 counted cells in total were identified to be FITC positive. The number of cells that interacted with the peptide increased only slightly with time, reaching $91\% \pm 6.9\%$ after 30 min of incubation. This indicated that the peptide rapidly interacts with *Candida* cells, confirming the measurements of membrane activity and our microscopic observations.

The distribution of the TB analog in the cytoplasm raised the question of how the peptide enters the yeast cell. We, therefore, exposed *C. albicans* to FITC-TB_KKG6K at its inhibitory concentration, applying conditions that reduced respiration and cellular metabolism, the aim being to discriminate between passive translocation and active, endocytic cell entry of the peptide. The yeast cells were incubated for 15 min with 2 μM peptide, either at 4°C, or at 30°C in the presence of 100 μM carbonyl cyanide *m*-chlorophenylhydrazone (CCCP), a chemical inhibitor of oxidative phosphorylation. Irrespective of the experimental setting, the peptide was always localized in the cytoplasm, similarly to cells incubated with the peptide at standard conditions (at 30°C without CCCP) (Fig. 6).

For comparison, we applied the *P. chrysogenum* antifungal protein B (PAFB), which was previously shown to require energy and active cellular metabolism to enter *C. albicans* cells (32). PAFB was conjugated with the green fluorophore 4,4-difluoro-5,7-dimethyl-4-bora-3a,4a-diaza-s-indacene-3-propionyl ethylenediamine hydrochloride (BODIPY) and incubated with the yeast cells at 30°C for 45 min. As expected, the labeled PAFB (BODIPY-PAFB) was taken up by *C. albicans* under these experimental conditions, but no internalization was observed in cells that had been exposed to BODIPY-PAFB at 4°C or in the presence of CCCP at 30°C (Fig. 6), proving that PAFB requires energy and active metabolism for cell entry.

This suggests that TB_KKG6K, unlike PAFB, enters yeast cells in an energy-independent manner when applied at its effective concentration.

TB_KKG6K disintegrates subcellular structures in *C. albicans*. Knowing that TB_KKG6K acts in a fungicidal way (7) and having localized the peptide in the cytoplasm of exposed cells, we performed electron microscopy of cryo-fixed cells to get an idea about the cellular damage induced in *C. albicans* by the application of a high concentration of the peptide. The submicroscopic architecture of the majority of untreated cells appeared intact (Fig. 7A and B), with all components known from budding yeasts (33) (Fig. 3). Nuclei, mitochondria, strongly stained vacuoles, late endosomes (multivesicular bodies [MVB]), endoplasmic reticulum (ER), ribosomes, and glycogen were constantly observed; peroxisomes (microbodies), elements of the inconspicuous Golgi apparatus, and small, endocytic or exocytic vesicles were present as well, albeit at lower frequencies. The exposure to TB_KKG6K caused severe ultrastructural damage to the vast majority of cells (Fig. 7C to G), except for a few morphologically intact individual cells (Fig. 7C, arrows). The most remarkable features, for example, were (i) heavy mitochondrial damage to the extent that those organelles (and their characteristic membrane architecture) were eventually hard to identify (Fig. 7D to G), (ii) disrupted nuclear envelope (Fig. 7F), (iii) increased frequency of late endosomes (MVB) (Fig. 7D), and (iv) strongly stained, partly irregularly shaped patches of ≈ 45 to 60 nm in width. In some cases, it was possible to identify such patches as membrane-bound, single or clustered vesicles, indicating endocytic traffic (Fig. 7D). Some patches likely represented glycogen rosettes and some

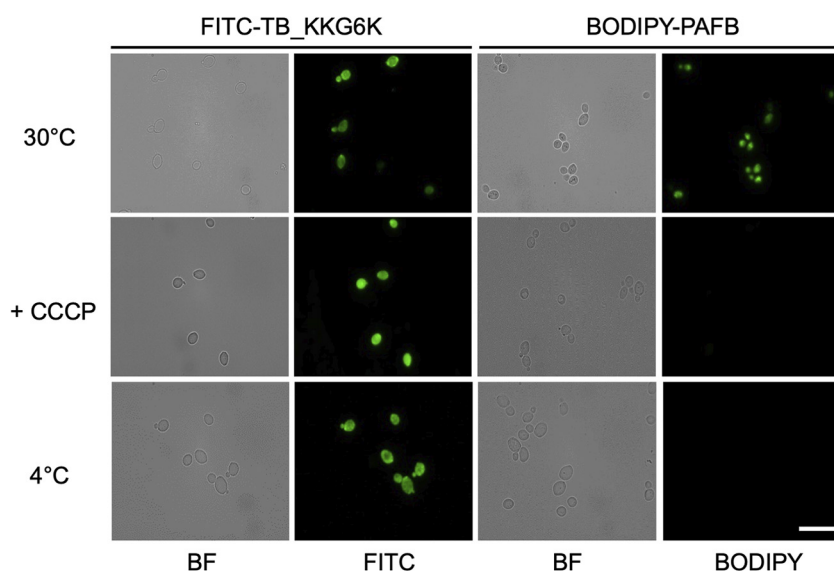


FIG 6 TB_KKG6K entry into *C. albicans* cells. Cells were exposed to 2 μ M FITC-TB_KKG6K for 15 min at 30°C (standard condition), at 30°C in the presence of 100 μ M CCCP (inhibition of respiration), or at 4°C (reduction of cellular metabolism) before fixation. As a control for energy-dependent uptake, *C. albicans* was incubated with 2 μ M BODIPY-PAFB for 45 min under the same incubation conditions as described above and then fixed for fluorescence microscopy. BF, bright-field microscopy; FITC, fluorescence microscopy. Scale bar, 15 μ m.

possibly aggregated polyribosomes; however, further work is needed for a more detailed characterization. Notably, the cellular shape of peptide-treated *C. albicans* along with the structure of its cell membrane and cell wall remained generally intact, and indications of cell lysis were not observed (Fig. 7C to G), with the possible exception of very sporadic, local cell membrane rupture (data not shown).

DISCUSSION

Recently, we reported for the first time that TB_KKG6K acts in a fungicidal manner against the opportunistic human yeast pathogen *C. albicans* (7). Previous studies on TB peptides and TB derivatives confirmed the ability of those compounds to inhibit bacterial growth due to their membrane-perturbing activity (9, 10, 34). The membrane activity of AMPs is hypothesized to play a significant role in the induction of expeditious killing of microbial cells (12, 35–37). Based on the high antifungal efficacy of TB_KKG6K at killing planktonic and sessile *C. albicans* cells *in vitro* (7), we focused, in the present study, on obtaining insights into the antifungal mechanism of action of this TB analog.

Using fluorescent dyes for the assessment of membrane depolarization [DiSC₃(5)] and permeabilization (SYTOX green), we showed that TB_KKG6K impaired cell membrane integrity. The TB analog induced an immediate depolarization and permeabilization of the fungal cell membrane in a concentration- and time-dependent manner (Fig. 1 and 2). Of note, the fluorescence intensity of depolarized cells in response to peptide exposure marginally decreased over time, after having reached a maximum value at 15 min with 1 μ M and 25 min with 2 μ M peptide, in contrast to the steadily increasing fluorescence intensity values of the positive control. This phenomenon might be due to the different ways by which the peptide (a nonlytic molecule) and Triton X-100 (lytic surfactant) act on the fungal cell. Due to peptide entry into the cell, the amount of membrane-bound TB_KKG6K available to depolarize the cell membrane might decrease with time. A similar trend was observed with AMPs and *C. albicans* by Gong et al. (38). It should also be considered that this fluorometric assay measures the average of a cell population containing polarized and depolarized cells, whereby the fluorescence intensity values might fluctuate depending on the heterogeneity of the cell population (15). In this respect, the formation of transient pores by the interaction of TB_KKG6K with the cell membrane could explain this scenario. In the case of Triton

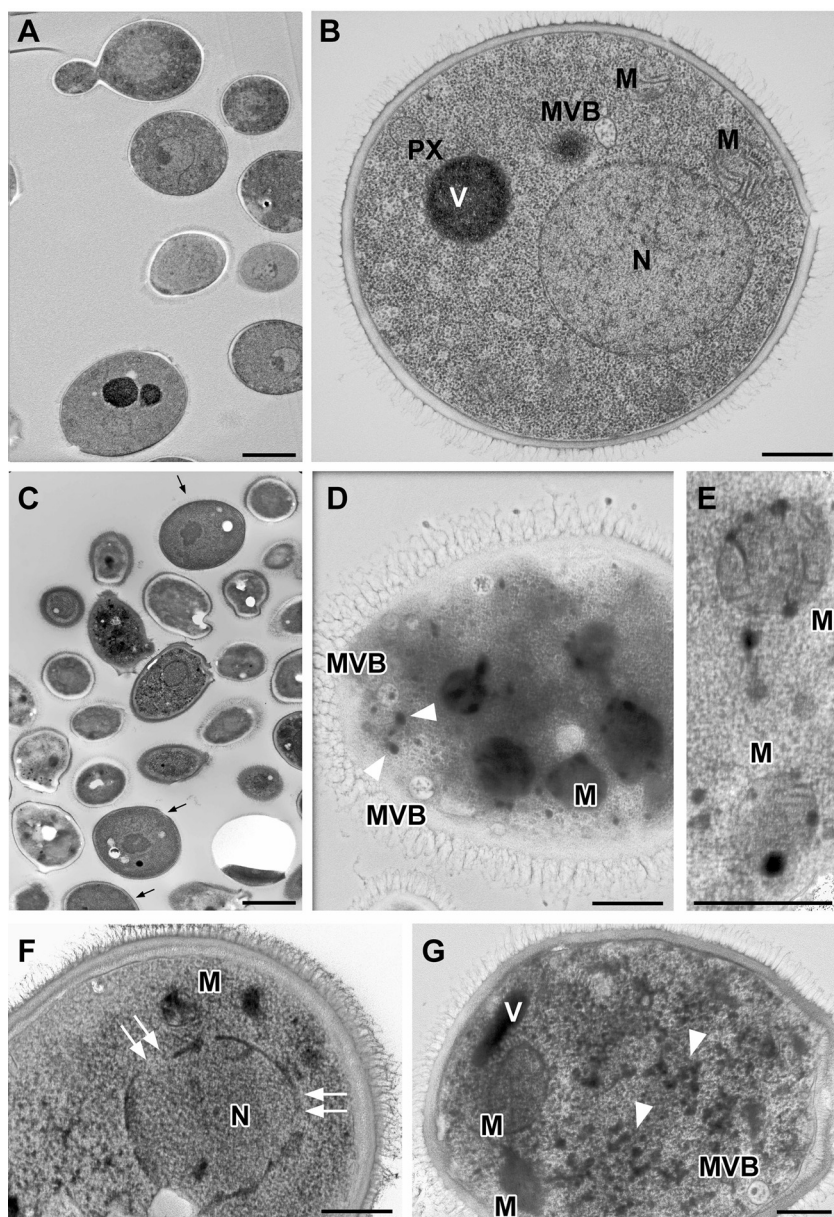


FIG 7 Changes in the cellular morphology of *C. albicans* in response to TB_KKG6K treatment. Electron micrographs of cryo-fixed *C. albicans* cells left untreated (controls) (A and B) or exposed to 30 μ M TB_KKG6K (C to G) at 30°C for 60 min. Scale bars, 2 μ m (A and C) or 500 nm (B, D, E, F, G). (A and B) Normal ultrastructure in untreated *C. albicans* serving as controls with nucleus (N), mitochondria (M), late endosomes (MVB), vacuoles (V), peroxisomes (PX), and abundant ribosomes and glycogen (not specifically highlighted) throughout the cytoplasm (the endoplasmic reticulum [ER] and Golgi apparatus are not depicted in those section planes). (C to G) Various patterns of subcellular degradation in TB analog-treated cells. (C) Overview showing only a few, visually intact cells (arrows). (D) Disintegrated mitochondria (M) are hardly recognizable, in contrast to numerous MVBs and strongly stained, small vesicles about 55 nm in width (arrowheads). (E) Damaged though recognizable mitochondria (M) with still-visible membrane remnants. (F) Ruptured envelope (double arrows) of the damaged nucleus (N). (G) Disintegrated mitochondria (M), MVB, and a vacuole (V), as well as strongly stained \approx 55-nm-wide patches (arrowheads), which are presumably (endocytic) vesicles and/or glycogen rosettes and/or ribosomal aggregates.

X-100, it cannot be ruled out that also cellular components released into the buffer upon cell lysis may interact with the DiSC₃(5) dye, stabilizing or even increasing the fluorescent signal (15).

The rapid reaction at the cell membrane does not allow any conclusion as to which of these two events - depolarization or permeabilization - precedes the other. Neither

membrane depolarization nor permeabilization is *per se* lethal as long as the cell is able to restore cell membrane function, e.g., under exposure to sublethal peptide concentrations (39). Cell membrane depolarization, however, often coincides with cell membrane permeabilization, resulting in severe membrane perturbation with excessive loss of ions and metabolite gradients due to membrane leakage or pore formation, affecting cell viability or even killing the cell by membrane rupture (40, 41). Persistent pores in the cell membrane and leakage of the cell content in response to exposure to TB_KKG6K, however, were not observed (Fig. 5 and 7). Therefore, the TB analog-induced cell membrane permeability is likely to be altered by a change in membrane structure, possibly by the establishment of transient pores that allow the nucleic acid binding dye SYTOX green to gain access into the cell (42–44). Also in this regard, the leakage of the low-MW compound ANTS-DPX from LUVs exposed to the TB analog is presumed to be the result of permeabilization but not rupture of the model membranes (45).

The use of model membranes containing different phospholipids and the quantification of the amount of ANTS-DPX dye leaking out from LUVs upon exposure to the TB analog revealed that TB_KKG6K induced leakage in LUVs composed of anionic PG (Table 1). This phospholipid represents the main component of membranes of Gram-positive bacteria (22). This was in agreement with the documented toxicity of the TB analog toward bacterial cells (10). However, the peptide also permeabilized LUVs containing the neutral lipid PC, proving that hydrophobic interactions play a role in its membrane activity. Neutral PC can be regarded as a primary building block of eukaryotic membranes, being one of the most abundant phospholipids in their lipid bilayer (26, 27). When comparing the effect of the TB analog on PC-LUVs with vesicles containing PC in combination with other specific membrane lipids, the leakage was significantly increased in the presence of PI, indicating that membranes containing this anionic phospholipid may be particularly amenable to TB_KKG6K attack (Table 1). Indeed, fungal cell membranes are generally more negatively charged than human ones due to a higher content of anionic phospholipids, such as PI and PA (12). This correlates with the results obtained from the peptide-lipid overlay experiments (Fig. 3). In this preliminary proof-of-principle experiment, TB_KKG6K showed preferential binding to unphosphorylated PI and PI mono-, bi-, and triphosphates (Fig. 3), which are known to play a crucial role in a number of cell membrane functions, including cell signaling and regulation of protein activity in and at the cell membrane (46, 47). Of particular significance is the negative charge of these phospholipids, which specifically attracts cationic AMPs (13, 48). It has to be noted, however, that PIP strip assays are based on the binding of peptides by virtue of their interactions with the head groups of lipids that are immobilized on a solid carrier (49). Therefore, these assays only have a limited informative value, as they do not reflect the complexity of cell membrane composition and structure, both of which have a strong impact on the peptide-lipid binding and membrane integrity (induction of leakage). As LUVs are membrane-mimetic vesicles tested in solution, they are closer to the *in vivo* scenario than PIP strips, because in leakage experiments intermolecular forces, such as electrostatic, hydrophobic, van der Waals, or hydrogen bonding, come into play with the peptide-lipid interaction.

This connection was exemplified with LUVs composed of only PC. Peptide exposure resulted in significant leakage of these LUVs, although the peptide-lipid overlay experiments showed no peptide binding to PC. This implied that the peptide was not able to interact with PC the way it did in the leakage assays.

Another lipid which, in combination with PC, increased LUV leakage at the highest peptide concentration tested was CL (Table 1), an integral mitochondrial membrane component (50, 51). This suggests that the peptide's activity is not restricted to the cell membrane but extends to intracellular targets, in this case, the mitochondrial envelope (52). Interestingly, in comparison to its effects on the membrane composed of only PC, TB_KKG6K evoked significantly lower leakage in PC-LUVs containing ergosterol or sphingomyelin, which are two lipids enriched in fungal (12, 53) and mammalian lipid

rafts (54–56), respectively. It has been reported that sterols, including ergosterol, reduce the membrane binding of AMPs such as LL-37 and Temporin L due to the sterols' ability to order themselves below the phospholipid head groups in the membrane. The resulting elevated acyl chain order and tightened lipid packing evokes increased membrane density and thickness (57). This improves the membrane stability, rendering it more difficult for AMPs to penetrate and insert themselves into the membrane, thereby conferring a certain degree of membrane protection for AMP attack (58, 59). The effect of sphingomyelin on AMP-induced membrane perturbation is comparatively less characterized; however, in line with our observation, the presence of sphingomyelin in model membranes reduces the membrane intercalation of LL-37, both alone and in combination with ergosterol (60). This, coupled with the fact that mammalian cell membranes are generally less negatively charged than fungal membranes, could also explain why TB_KKG6K is well tolerated by primary human cells *in vitro* (7). The question of whether any of the lipids identified to increase the leakage of LUVs by the TB analog represent potential direct peptide targets, or render the membrane susceptible to peptide-lipid interactions, awaits further investigations in the future.

Physicochemical investigations on a number of AMPs and cell-penetrating peptides have demonstrated that, apart from charge and amphipathicity, their secondary structure and conformation play a crucial role in their ability to interact with cellular membranes (38, 61, 62). In particular, circular dichroism spectroscopy studies revealed a characteristic shift from a random, disordered secondary structure of TB_KKG6K in an aqueous environment to an α -helical conformation in the presence of sodium dodecyl sulfate, a fungal cell membrane surface mimetic (7). This structural transition is hypothesized to facilitate binding and insertion of peptides into the fungal cell membrane (38, 63, 64). The *in silico* helical-wheel projection studies underlined these data (Fig. 4). Compared to the membrane-active anti-*Candida* peptide LL-37₁₃₋₃₇ (28), the predicted α -helix of TB_KKG6K showed greater potential for its insertion into the hydrophobic portion of the membrane bilayer (Fig. 4). This model was further supported by the calculated membrane-partitioning free energy and the hydrophobic moment, which were both lower for the TB analog compared to those for LL-37₁₃₋₃₇ (Fig. 4).

The conclusion that TB_KKG6K perturbs the fungal cell membrane and, in terms of energetics, can penetrate the cell membrane with relative ease, was proven by fluorescence microscopy with a FITC-labeled TB_KKG6K. Costaining with the lipophilic dye FM4-64 (65) helped us follow the entry of the peptide into the fungal cell (Fig. 5). The exposure to FITC-TB_KKG6K at its IC₉₀, however, immediately impaired cell membrane integrity and disrupted the specific membrane binding capability of FM4-64, causing the lipophilic dye to spread across the cell and colocalize with the peptide-specific fluorescent signal in the cytoplasm (Fig. 5). Overview images confirmed that only those cells that had internalized the peptide presented a diffuse FM4-64 staining pattern (see Fig. S1 in the supplemental material). The peptide action, however, was too rapid to capture the presumed initial colocalization of FITC-TB_KKG6K with FM4-64 in the cell membrane prior to peptide-associated cell membrane perturbation. The swift manner with which the peptide interacted with over 89% of the cells within a very short time of exposure was confirmed by FACS-based quantification of FITC-positive cells. In contrast, the membrane affinity and distinct compartmentalization in presumptive vacuoles of FITC-TB_KKG6K were occasionally visible in the cells that had been exposed to subinhibitory peptide concentrations (Fig. 5). Several possible explanations might account for this observation. (i) Peptide entry into the cell is concentration dependent, as has been shown for other AMPs like the hexapeptide PAF26 (66), Histatin-5 (67), or pVEC (68). At subinhibitory concentrations, these peptides are internalized by receptor-mediated endocytosis and accumulate in the vacuole, while they directly translocate into the cytoplasm of the target cell at their effective concentration, inducing cell death. (ii) The concentration of the TB analog has no influence on the mode of internalization, and cellular entry always occurs in an energy-independent manner. Interestingly, Maniti et al. described a hypothesized "energy-independent endocytic process" that allows the cell-penetrating peptide "penetratin" to

induce membrane curvature in artificial lipid membranes due to its positive charge (69). If the angle of curvature crosses a certain threshold, it could cause the membrane to fold back upon itself, forming a peptide-containing, endosome-like invagination and facilitating peptide uptake independent of energy (69). If the mode of TB_KKG6K entry into yeast cells takes place in a similar manner, the uptake of the peptide at subinhibitory concentrations and its dispersion from the vacuole into the cytoplasm would occur slower than at the effective concentration, which would allow the vacuolar localization of the peptide to be observed microscopically. The question of how TB_KKG6K enters the fungal cell certainly merits further investigations. In contrast to PAFB, however, which is internalized via endocytosis (32), the entry of TB_KKG6K into *C. albicans* cells at the peptide's effective concentration was hampered neither by the reduction of cellular metabolism nor by the inhibition of oxidative phosphorylation, excluding the involvement of a receptor-mediated endocytic pathway at this concentration (Fig. 6). Passive entry into microbial cells is considered more advantageous in terms of antimicrobial efficacy, as energy-dependent AMPs easily lose their activity under physiological conditions of reduced metabolic activity, e.g., in cells growing in a biofilm (70–72). The accumulation of FITC-TB_KKG6K in the vacuole, when applied at subinhibitory peptide concentrations, might also protect the cells from peptide-induced cell death. In fact, a similar phenomenon has been observed with many AMPs (12, 66, 67), including the *P. chrysogenum* antifungal proteins PAF, PAFB, and PAFC (73, 74). The induction of cell death was closely linked with the cytoplasmic localization of the AMPs, but it did not take place as long as the peptides resided in the vacuole. Either these peptides are degraded, or they overcome vacuolar function; with the latter scenario, it is then only a matter of time until they disrupt the vacuolar membrane, spread into the cytoplasm, and kill the cell.

Finally, transmission electron microscopy revealed a severe disintegration of intracellular structures in response to the treatment of *C. albicans* cells with TB_KKG6K (Fig. 7). Although the cell content was heavily damaged, the overall cell shape was retained and the structure of the cell wall and the cell membrane showed no signs of lysis in the presence of the TB analog (Fig. 7). The substantial intracellular damage observed in response to cellular exposure to TB_KKG6K could be the consequence of the peptide's permeabilizing effects on the cell membrane resulting in dysregulated ion and metabolite homeostasis. Furthermore, since TB_KKG6K translocated into the cell and intracellular membranes contain high amounts of anionic phospholipids and PIPs, it is reasonable to assume that the peptide also interacted with the subcellular membranes, damaging them and disrupting organelle function, e.g., mitochondria and nuclei (Fig. 7). Another explanation could be that the peptide interacts with intracellular components apart from lipids (e.g., proteins, nucleic acids) that are equally crucial to maintain the cellular structure and function. Addressing this possibility in more detail will be the scope of further studies. The ability of TB_KKG6K to permeabilize model membranes containing CL (Table 1) suggests that the peptide interacts with the inner mitochondrial membrane, where CL resides. Impairment of CL function and/or mitochondrial damage by the TB analog could disturb respiration and the regulation of reactive oxygen species (ROS) generation (50). This could be one reason for the peptide's observed induction of intracellular ROS (7), which is known to damage cellular organelles and molecules, including nucleic acids, proteins, and lipids (13, 75).

Conclusion. Our study provides a rationale behind the rapid killing of *C. albicans* by TB_KKG6K. Based on our results, we propose the following model to explain its mechanism of action. The TB analog preferentially affects membranes composed of anionic but also neutral phospholipids. Due to its physicochemical features (charge, hydrophobicity), we assume that TB_KKG6K binds to the yeast cell membrane via hydrophobic interactions, whereby additional electrostatic interactions with the anionic heads of membrane lipids stabilize the peptide-lipid binding. Upon cell membrane binding, the peptide impairs the integrity of the cell membrane. Membrane depolarization and permeabilization might facilitate the peptide's translocation

through the membrane into the cell, where it interacts with intracellular targets and directly or indirectly executes its killing activity (76). The translocation of the TB analog into the yeast cell, its intracellular distribution, and the disintegration of subcellular structures but not that of the cell wall or the cell membrane further underlines that TB_KKG6K is a membrane-active, nonlytic peptide that also affects the membrane integrity of intracellular compartments, possibly in combination with the direct and/or indirect induction of intracellular ROS. The documented mode of action renders this peptide a promising candidate for the development of next-generation anti-*Candida* therapeutics. Due to its rapid, fungicidal activity, this amphibian peptide analog may hamper the onset of drug resistance, which has become increasingly challenging in the treatment of mycoses caused by the opportunistic human pathogen *C. albicans*.

MATERIALS AND METHODS

Microorganisms, media, and growth conditions. Single, fresh colonies of *C. albicans* (CBS 5982) grown on solid yeast extract-peptone-dextrose agar (yeast extract peptone dextrose broth [YPDB] with 2% [wt/vol] agar; Sigma-Aldrich, St. Louis, MO, USA) were used to inoculate 10 mL of YPDB. After overnight cultivation at 37°C and shaking at 200 rpm, the cells were counted and diluted in 5% (wt/vol) potato dextrose broth (0.05× PDB) to the cell number applied in the respective experiments described below.

Peptide synthesis and protein expression. TB_KKG6K and PC γ ^{C-terminal} were synthesized on solid phase, using standard protocols for the 9-fluorenylmethoxy chemistry and were then purified by reversed-phase high-performance liquid chromatography (RP-HPLC) and analyzed by electrospray ionization-mass spectrometry (ESI-MS) as described previously (7, 14). For fluorescence-based analyses, the TB analog was synthesized and conjugated to the 6-aminohexanoic acid linker first and then to the green fluorophore FITC as described elsewhere (77). The FITC-conjugated peptide (FITC-TB_KKG6K) was purified by RP-HPLC on a Jupiter 10- μ m Proteo 90A° (100 × 21, 20 mm) column, with a flow rate 20.0 mL/min, and analyzed by ESI-MS as described by Kakar et al. (7): calculated mass (Da), 2221.28; found, 1111.88 [M + 2H]²⁺; 741.82 [M + 3H]³⁺. The *P. chrysogenum* antifungal protein PAFB was expressed using a *P. chrysogenum*-based expression system (78) and purified by cation-exchange chromatography as previously described (32). For fluorescence-based analyses, PAFB was labeled with the green fluorophore BODIPY FL EDA (Invitrogen, Waltham, MA, USA) as described previously (32).

Broth microdilution assays. The IC₉₀ values of the TB analog octenidine (Schülke and Mayr GmbH, Vienna, Austria) and PC γ ^{C-terminal} (14) were determined for *C. albicans* using broth microdilution assays carried out in 96-well microtiter plates (Nunclon Delta, Thermo Fisher Scientific, Waltham, MA, USA). The assay was performed with 1 × 10⁴ cells/mL and 1 × 10⁶ cells/mL in 0.05× PDB. Briefly, 100 μ L of either cell concentration was mixed with 100 μ L of 2-fold compound dilutions prepared in 0.05× PDB in a 96-well microtiter plate. The final concentration range of the compounds tested was 0 to 32 μ M. The plates were incubated at 30°C for 24 h under static conditions. The cells were then resuspended by vigorous pipetting, and the optical density (OD) of the resuspended cell suspension was measured with a multimode microplate reader (FLUOstar Omega, BMG Labtech, Ortenberg, Germany) at a wavelength of 620 nm. The OD₆₂₀ of the untreated control was assigned 100% growth. All samples were prepared in technical triplicates, and the assays were repeated at least twice.

Membrane depolarization assay. *C. albicans* cells were prepared in 0.05× PDB at a concentration of 1 × 10⁶ cells/mL, and 100 μ L was added to each well of a black polystyrene microtiter plate (Greiner Bio-One, Frickenhausen, Germany). Fluorescence intensity was followed for 7 min 30 s at an excitation/emission wavelength of 622/670 nm using a multimode microplate reader (CLARIOstar Plus, BMG Labtech, Ortenberg, Germany) to obtain baseline values for cell and medium background fluorescence. Measurements of the fluorescence intensity were then paused, and 50 μ L of DiSC₃(5) dye (Thermo Fisher Scientific, Waltham, MA, USA), prepared separately in 0.05× PDB at a concentration of 6 μ M, was added to each well. Fluorescence measurements were continued until a stable signal was achieved. Serial dilutions of the TB analog Triton X-100 (positive control) and PC γ ^{C-terminal} (negative control) were prepared in 0.05× PDB in a separate 96-well microtiter plate (Nunclon Delta; Thermo Fisher Scientific) in a final volume of 50 μ L per well. For the untreated control, 50 μ L of 0.05× PDB replaced compound addition. Measurements of the fluorescence intensity were paused, and 50 μ L of the serially diluted compounds were added to the cell suspension, resulting in a final volume of 200 μ L per well and a final DiSC₃(5) concentration of 1.5 μ M. The final concentrations of the positive and negative controls were 1% (wt/vol) and 32 μ M, respectively. The TB analog was tested at a final concentration range of 0 to 2 μ M. The fluorescence intensity measurements were recommenced after compound addition and were recorded at 30°C in 5-min intervals for a further 60 min. The fluorescence values obtained post-compound addition were background-corrected (sample without cells) and normalized by subtracting the values of the untreated control from the values of the treated samples.

SYTOX green uptake assay. *C. albicans* cells were prepared in 0.05× PDB at a concentration of 1 × 10⁶ cells/mL. The SYTOX green nucleic acid stain (Thermo Fisher Scientific, Waltham, MA, USA) was then added to the cell suspension at a final concentration of 0.2 μ M. The cells were incubated in the dark at 30°C for 5 min under static conditions. In the meantime, serial dilutions of the TB analog, the positive

control octenidine, and the negative control PC γ ^{C-terminal} were prepared in 0.05× PDB in a 96-well microtiter plate (Nunc Delta; Thermo Fisher Scientific) at a volume of 100 μ L per well. The cell suspension, after preincubation with SYTOX green, was distributed in 100- μ L aliquots per well in the compound-containing 96-well microtiter plate (Nunc Delta; Thermo Fisher Scientific). The final concentrations of the positive and negative controls were 2 μ M and 32 μ M, respectively. The TB analog was tested at a final concentration range of 0 to 2 μ M. For the untreated control, 0.05× PDB replaced compound addition. As an additional control, SYTOX green was combined with the compounds (TB analog, octenidine, PC γ ^{C-terminal}) in their respective concentrations, as well as with the assay medium without compounds, all in the absence of cells. Fluorescence intensities were measured in 5-min intervals for 60 min at 30°C using an excitation/emission wavelength of 480/530 nm in a multimode microplate reader (CLARIOstar Plus, BMG Labtech, Ortenberg, Germany). The fluorescence values were first background-corrected by subtracting the arbitrary fluorescence unit (AFU) values of the SYTOX green combined with and without the compounds (peptide, octenidine, PC γ ^{C-terminal}), all in the absence of cells, from the respective AFU values obtained in the presence of cells. This was done for each peptide concentration (0.5 μ M, 1 μ M, 2 μ M) and for the controls octenidine and PC γ ^{C-terminal}. The background-corrected AFU values were then normalized by subtracting the AFU values of the untreated control (SYTOX green with cells).

Lipid-peptide overlay assay. The lipid-peptide overlay assay was performed using FITC-conjugated TB_KKG6K and PIP strips according to the manufacturer's instructions (Echelon Biosciences, Salt Lake City, UT, USA). To ensure the suitability of the applied detection method, 0.5 μ g of FITC-TB_KKG6K was directly dotted in a volume of 1 μ L onto the PIP strip membranes. The dotted peptide was allowed to dry for 30 min at 30°C before the PIP strips were tested with FITC-TB_KKG6K. Briefly, the PIP strips were blocked in blocking buffer (10 mM Tris [pH 8.0], 150 mM NaCl, 0.1% [wt/vol] Tween 20, 3% [wt/vol] fatty acid-free bovine serum albumin; Sigma-Aldrich, St. Louis, MO, USA) for 1 h. All of the subsequent experimental procedures were performed in the dark. The PIP strips were incubated for 1 h with FITC-TB_KKG6K and diluted in blocking buffer to a final concentration of 1.5 μ g/mL. Then, the membranes were washed three times for 10 min each in blocking buffer. The FITC-TB_KKG6K binding to specific PIs was detected fluorometrically with a Typhoon FLA 9500 biomolecular imager (GE Healthcare, Chicago, IL, USA) equipped with a 473-nm laser and filters for excitation/emission wavelengths of 494/520 nm. The FITC fluorescence signal intensity was semiquantified by ImageJ/FIJI software (version 1.8.0/1.53q; U.S. National Institutes of Health, Bethesda, MD, USA).

Vesicle leakage assay. For the leakage experiments, the following lipids were used: 1-palmitoyl-2-oleoyl-glycero-3-phosphocholine (PC), 1-palmitoyl-2-oleoyl-*sn*-glycero-3-phosphoethanolamine (PE), 1',3'-bis[1,2-dioleoyl-*sn*-glycero-3-phospho]-glycerol, sodium salt (cardiolipin [CL]), egg sphingomyelin, 1-palmitoyl-2-oleoyl-*sn*-glycero-3-[phospho-*rac*-(1-glycerol)] (PG), 1-palmitoyl-2-oleoyl-*sn*-glycero-3-phosphoinositol, ammonium salt (PI), 1-palmitoyl-2-oleoyl-*sn*-glycero-3-phospho-L-serine, sodium salt (PS), ergosterol, *N*-palmitoyl-D-erythro-sphingosine (ceramide). All lipids were purchased from Avanti Polar Lipids (Alabaster, AL, USA).

Lipid films composed of PC, PG, PC-PI (9:1 mol), PC-PS (9:1 mol), PC-PE (9:1 mol), PE-PG-CL (6:2:1 mol), PC-ergosterol (4:1 mol), PC-ceramide (9:1 mol), PC-CL (3:1 mol), PC-sphingomyelin (9:1 mol), PC-PE-ergosterol (PC-PE at 9:1 mol, PC-PE-ergosterol at 4:1 mol), and PC-PS-ergosterol (PC-PS at 9:1 mol; PC-PS-ergosterol at 4:1 mol) were prepared by dissolving the appropriate lipids, prepared in glass tubes at a total amount of 20 mg, in chloroform-methanol (2:1 [vol/vol]). The glass tubes were subsequently placed under a stream of nitrogen to allow the solvent to evaporate. They were then stored under vacuum overnight to completely remove all residual traces of solvent.

The prepared lipid films were hydrated in 10 mM HEPES buffer (pH 7.4) containing 68 mM NaCl, 12.5 mM ANTS (Molecular Probes, Eugene, OR, USA), and 45 mM DPX (Molecular Probes, Eugene, OR, USA). The hydration process was carried out with intermittent vortexing for 1 min at the time points 0, 5, 10, 20, 30, and 60 min. For each formulation, a temperature well above the gel-to-fluid phase transition of its constituent lipids was applied. The hydrated lipid films were then extruded 25 times using a handheld mini extruder (Avanti Polar Lipids, Alabaster, AL, USA) with a 100-nm-pore-diameter polycarbonate filter to obtain 100-nm LUVs. Unilamellarity and size were confirmed by dynamic light scattering using a Zetasizer Nano system (ZSP; Malvern Analytical, Prager Electronics, Wolkersdorf, Austria).

The ANTS-DPX-containing LUVs were separated from free ANTS-DPX by exclusion chromatography using a column filled with Sephadex G-75 fine gel (Amersham Biosciences, Amersham, United Kingdom) swollen in an isotonic buffer (10 mM HEPES, 140 mM NaCl; pH 7.4). After the void volume, fractions were collected and the phospholipid concentration was determined by phosphate analysis as described by Piller et al. (79). The LUVs containing ANTS-DPX were stored in the dark at room temperature.

The leakage of aqueous contents from the prepared LUVs induced by the TB analog was determined using the GloMax Discover microplate reader (Promega Corporation, Madison, WI, USA). Briefly, serial dilutions of the peptide were prepared in HEPES buffer (10 mM HEPES, 140 mM NaCl; pH 7.4) in a black 96-well microtiter plate (Nunc Delta, Thermo Fisher Scientific, Waltham, MA, USA) in a final volume of 10 μ L per well. Ninety microliters of the respective LUVs was added to each well, resulting in a final lipid concentration of 50 μ M in a final volume of 100 μ L per well. For the untreated lipid control, 10 μ L of HEPES buffer was used instead of the peptide. Ten microliters of 10% (wt/vol) Triton X-100 was used as the positive control. The peptide PC γ ^{C-terminal} was used as a negative control at a final concentration of 32 μ M. The leakage measurements were started immediately after LUV addition. Fluorescence spectra were obtained at 37°C over a period of 90 min using an excitation/emission wavelength of 360/530 nm. Data are presented in terms of percent leakage and were calculated using the following equation: % leakage = $[(F - F_0)/(F_{\max} - F_0)] \times 100$, where F is the measured fluorescence, F_0 is the fluorescence with

only the lipid (untreated control), and F_{\max} is the fluorescence corresponding to 100% leakage obtained by the addition of 1% (wt/vol) Triton X-100.

Evaluation *in silico* of peptide-membrane binding. Totalizer, a tool provided by Membrane Protein Explorer mPEX v3.3.0, was used to characterize the binding of TB_KKG6K in comparison to the reference peptide LL-37 (amino acid sequence LLGDFFRKSKEK**IGKEFKRIVQRIKDFLRNLLVPRTE**S; MW, 4,493.3 Da) (28) to the lipid membrane-water interface (31). For the latter, amino acids 13 to 37, marked in bold, were considered for analysis. The *in silico* helical wheel projection, bilayer partitioning free energy (ΔG), and hydrophobic moment (μ) were obtained as described by Piller et al. (79). For ΔG , values were calculated using the octanol scale, which calculates the free energy of peptide transfer from water to the hydrophobic region of the membrane bilayer to that of octanol.

Assessment of the cellular localization and uptake mechanism of TB_KKG6K. To follow the sub-cellular distribution, two different strategies were pursued using the FITC-conjugated TB_KKG6K. In the first approach, 2 μ M FITC-TB_KKG6K was added along with 5 μ M of the cell wall-specific fluorescent dye calcofluor white (CFW; Sigma-Aldrich, St. Louis, MO, USA) to 800 μ L of the *C. albicans* cell suspension (1×10^6 cells/mL in $0.05 \times$ PDB) and incubated with the cells for 15 min at 30°C in the dark to determine if the conjugate localized with the fungal cell wall. The cell suspension was then washed once with phosphate-buffered saline (PBS; 0.5% [wt/vol] KH_2PO_4 , 2.8% [wt/vol] K_2HPO_4 , 9% [wt/vol] NaCl) and fixed in 100 μ L of 4% (vol/vol) formaldehyde (FA; Carl Roth GmbH & Co., Karlsruhe, Germany) for 10 min. The FA was removed by washing with PBS, and 2×10^5 cells (in $0.05 \times$ PDB) per well were transferred to ibidi μ -slide 8-well chambered coverslips (Ibidi GmbH, Gräfelfing, Germany) for microscopy.

The second set of experiments was performed to assess the *in vivo* membrane binding of the peptide and its cellular distribution. To this end, 2×10^5 *C. albicans* cells (in $0.05 \times$ PDB) per well were distributed in ibidi μ -slide 8-well chambered coverslips and stained with 0.8 μ M of the membrane-specific fluorescent styryl dye FM4-64 (Thermo Fisher Scientific, Waltham, MA, USA) in the absence (control) and presence of 0.5 μ M, 1 μ M and 2 μ M of FITC-TB_KKG6K. Live cell imaging, performed at 30°C, started immediately after compound addition.

For imaging both approaches, LSM was carried out using an HC PL APO 40 \times /1.10 CS2 water immersion objective on an SP8 confocal microscope (Leica Microsystems, Wetzlar, Germany) equipped with an 80-MHz pulsed white light laser (WLL) and a 405-nm CW diode laser. HyD detectors were used for optical fluorescence imaging. Images of CFW (excitation, 405 nm diode; emission, 415 to 479 nm), FITC-TB_KKG6K (excitation, 495 nm WLL; emission, 515 to 530 nm), and FM4-64 (excitation, 515 nm WLL; emission, 670 to 700 nm) were acquired using the Leica Application Suite X (LAS X; version 3.5.7.23225) and further processed by ImageJ/FIJI.

To study the uptake mechanism into the yeast cells, 2 μ M FITC-TB_KKG6K was added to 400 μ L of a *C. albicans* cell suspension (1×10^6 cells/mL in $0.05 \times$ PDB) and incubated for 15 min at 30°C in the dark. To uncouple mitochondrial oxidative phosphorylation, the cells were incubated with 100 μ M CCCP (Sigma-Aldrich, St. Louis, MO, USA) in the presence of FITC-TB_KKG6K, applying the same incubation conditions. The metabolic activity of the cells was reduced by incubating the cells with FITC-TB_KKG6K at 4°C instead of 30°C. For comparison with an AMP that is taken up by *C. albicans* in an energy-dependent way, PAFB conjugated with the fluorophore BODIPY (BODIPY-PAFB), prepared as described previously (32), was used. In brief, cells were exposed to 2 μ M BODIPY-PAFB, applying the same experimental conditions as described above. After 45 min of incubation, the cells were washed in PBS and fixed in 100 μ L 4% (vol/vol) FA for 10 min. After washing in PBS, the cells were mounted on glass slides for microscopic analysis. Microscopic imaging of these samples was performed with a fluorescence microscope (Axioplan; Carl Zeiss GmbH, Oberkochen, Germany), equipped with excitation/emission filters (500/535 nm or 450/515 nm for BODIPY or FITC, respectively) and an AxioCam MR3 camera (Carl Zeiss GmbH, Oberkochen, Germany). The images were processed and edited with Axiovision (blue edition), GNU Image Manipulation Program (GIMP, version 2.8.20; www.gimp.org), and Microsoft PowerPoint software.

Ultrastructural analysis of *C. albicans*. For electron microscopy, 3×10^8 *C. albicans* cells in 1 mL of $0.05 \times$ PDB were exposed to 30 μ M TB_KKG6K for 1 h at 30°C under continuous shaking. Untreated cells served as a control. Cell suspensions were slightly pelleted and subjected to rapid cryo-fixation by means of high-pressure freezing and freeze-substitution, followed by epoxy resin embedding essentially as previously described (80), except that the freeze-substitution medium contained only 0.8% (wt/vol) uranyl acetate. Thin sections were optionally poststained with lead salts and viewed with a CM120 transmission electron microscope (Philips, Eindhoven, The Netherlands) equipped with a MORADA digital camera (EMSI, Münster, Germany).

Fluorescence-activated cell sorting. *C. albicans* cells were diluted to 4×10^6 cells/mL in $0.05 \times$ PDB, and 100 μ L of this cell suspension was exposed to 100 μ L of FITC-TB_KKG6K prepared in $0.05 \times$ PDB to reach a final peptide concentration of 2 μ M. The cells were incubated in the dark for 5 or 30 min at 30°C under static conditions. Untreated cells were used as the negative control. After peptide exposure, the cells were pelleted ($900 \times g$ for 5 min) and washed twice in PBS. At least 5,000 cells were counted per run, and FITC-positive cells were detected with a FlowSight imaging flow cytometer (Amins; Merck Millipore, Billerica, MA, USA) equipped with lasers at 405 nm (violet), 488 nm (blue), and 642 nm (red) wavelengths. The FITC signal was measured utilizing a 488-nm excitation laser and emission in the channel 2 window. Gating was adjusted to reach at least 99% of untreated cells; debris was excluded during data acquisition. For data analysis, the Image Data Exploration and Analysis software (IDEAS; Amins, Millipore, Billerica, MA, USA) was applied. Experiments were repeated three times.

Statistical analysis. For calculation of significant differences, two-way analysis of variance (ANOVA) followed by Dunnett's multiple-comparison test was performed using GraphPad Prism version 9.1.0 for macOS. *P* values of ≤ 0.05 were considered significant.

SUPPLEMENTAL MATERIAL

Supplemental material is available online only.

FIG S1, TIF file, 2.6 MB.

FIG S2, TIF file, 2.3 MB.

ACKNOWLEDGMENTS

F.M. and N.M. designed the experiments and conceived and supervised the study. A.K. performed experiments, and A.K., N.M., and F.M. analyzed the data. L.E.S.-V. performed laser scanning microscopy. M.H. performed electron microscopy. L.G. and C.P. performed FACS analysis. J.H. prepared the samples for electron microscopy, and A.R. provided TB_KKG6K. G.V. provided PCy^{C-terminal}. A.K. prepared the first manuscript draft. All authors contributed to manuscript writing and revision and approved the submitted version.

We thank W. Salvenmoser for helpful discussion, and D. Bratschun-Khan, K. Gutleben, and B. Witting for technical assistance. The study was funded by the Austrian Science Fund FWF (HOROS Doctoral Program, W1253 DK HOROS) to F.M. and L.G. was financed by the Hungarian National Research, Development and Innovation Office (NKFIH, FK 134343 project).

We have no conflict of interest to declare.

REFERENCES

- Garber G. 2001. An overview of fungal infections. *Drugs* 61(Suppl 1):1–12. <https://doi.org/10.2165/00003495-200161001-00001>.
- Lee DJ, O'Donnell H, Routier FH, Tiralongo J, Haselhorst T. 2019. Glycobiology of human fungal pathogens: new avenues for drug development. *Cells* 8:1348. <https://doi.org/10.3390/cells8111348>.
- Kainz K, Bauer MA, Madeo F, Carmona-Gutierrez D. 2020. Fungal infections in humans: the silent crisis. *Microb Cell* 7:143–145. <https://doi.org/10.15698/mic2020.06.718>.
- Talapko J, Juzbašić M, Matijević T, Pustijanac E, Bekić S, Kotris I, Škrlec I. 2021. *Candida albicans*: the virulence factors and clinical manifestations of infection. *J Fungi (Basel)* 27:79. <https://doi.org/10.3390/jof7020079>.
- do Nascimento Dias J, de Souza Silva C, de Araújo AR, Souza JMT, de Holanda Veloso Júnior PH, Cabral WF, da Glória da Silva M, Eaton P, de Souza de Almeida Leite JR, Nicola AM, Albuquerque P, Silva-Pereira I. 2020. Mechanisms of action of antimicrobial peptides ToAP2 and NDBP-5.7 against *Candida albicans* planktonic and biofilm cells. *Sci Rep* 10:10327. <https://doi.org/10.1038/s41598-020-67041-2>.
- Fernández de Ullivarri M, Arbulu S, Garcia-Gutierrez E, Cotter PD. 2020. Antifungal peptides as therapeutic agents. *Front Cell Infect Microbiol* 10:105. <https://doi.org/10.3389/fcimb.2020.00105>.
- Kakar A, Holzknacht J, Dubrac S, Gelmi ML, Romanelli A, Marx F. 2021. New perspectives in the antimicrobial activity of the amphibian Temporin B: peptide analogs are effective inhibitors of *Candida albicans* growth. *J Fungi* 7:457. <https://doi.org/10.3390/jof7060457>.
- Mangoni ML, Marcellini HG, Simmaco M. 2007. Biological characterization and modes of action of temporins and bombinins H, multiple forms of short and mildly cationic anti-microbial peptides from amphibian skin. *J Pept Sci* 13:603–613. <https://doi.org/10.1002/psc.853>.
- Avitabile C, Netti F, Orefice G, Palmieri M, Nocerino N, Malgieri G, D'Andrea LD, Capparelli R, Fattorusso R, Romanelli A. 2013. Design, structural and functional characterization of a Temporin-1b analog active against Gram-negative bacteria. *Biochim Biophys Acta* 1830:3767–3775. <https://doi.org/10.1016/j.bbagen.2013.01.026>.
- Avitabile C, D'Andrea LD, D'Aversa E, Milani R, Gambari R, Romanelli A. 2018. Effect of acylation on the antimicrobial activity of Temporin B analogues. *ChemMedChem* 13:1549–1554. <https://doi.org/10.1002/cmdc.201800289>.
- Bezzerri V, Avitabile C, Dechechchi MC, Lampronti I, Borgatti M, Montagner G, Cabrini G, Gambari R, Romanelli A. 2014. Antibacterial and anti-inflammatory activity of a temporin B peptide analogue on an *in vitro* model of cystic fibrosis. *J Pept Sci* 20:822–830. <https://doi.org/10.1002/psc.2674>.
- Rautenbach M, Troskie AM, Vosloo JA. 2016. Antifungal peptides: to be or not to be membrane active. *Biochimie* 130:132–145. <https://doi.org/10.1016/j.biochi.2016.05.013>.
- Struyfs C, Cammue BPA, Thevissen K. 2021. Membrane-interacting anti-fungal peptides. *Front Cell Dev Biol* 9:649875. <https://doi.org/10.3389/fcell.2021.649875>.
- Czajlik A, Holzknacht J, Galgóczy L, Tóth L, Poór P, Ördög A, Váradi G, Kühbacher A, Borics A, Tóth GK, Marx F, Batta G. 2021. Solution structure, dynamics, and new antifungal aspects of the cysteine-rich miniprotein PAFC. *Int J Mol Sci* 22:1183. <https://doi.org/10.3390/ijms22031183>.
- Te Winkel JD, Gray DA, Seistrup KH, Hamoen LW, Strahl H. 2016. Analysis of antimicrobial-triggered membrane depolarization using voltage sensitive dyes. *Front Cell Dev Biol* 4:29. <https://doi.org/10.3389/fcell.2016.00029>.
- Roth BL, Poot M, Yue ST, Millard PJ. 1997. Bacterial viability and antibiotic susceptibility testing with SYTOX green nucleic acid stain. *Appl Environ Microbiol* 63:2421–2431. <https://doi.org/10.1128/aem.63.6.2421-2431.1997>.
- Koburger T, Hübner NO, Braun M, Siebert J, Kramer A. 2010. Standardized comparison of antiseptic efficacy of triclosan, PVP-iodine, octenidine dihydrochloride, polyhexanide and chlorhexidine digluconate. *J Antimicrob Chemother* 65:1712–1719. <https://doi.org/10.1093/jac/dkq212>.
- Islam KT, Velivelli SLS, Berg RH, Oakley B, Shah DM. 2017. A novel bi-domain plant defensin MtDef5 with potent broad-spectrum antifungal activity binds to multiple phospholipids and forms oligomers. *Sci Rep* 7:16157. <https://doi.org/10.1038/s41598-017-16508-w>.
- Ladokhin AS, Wimley WC, White SH. 1995. Leakage of membrane vesicle contents: determination of mechanism using fluorescence reequenching. *Biophys J* 69:1964–1971. [https://doi.org/10.1016/S0006-3495\(95\)80066-4](https://doi.org/10.1016/S0006-3495(95)80066-4).
- Samuel R, Gillmor S. 2016. Membrane phase characteristics control NA-CATH activity. *Biochim Biophys Acta* 1858:1974–1982. <https://doi.org/10.1016/j.bbamem.2016.05.015>.
- Apellániz B, Nieva JL, Schwille P, García-Sáez AJ. 2010. All-or-none versus graded: single-vesicle analysis reveals lipid composition effects on membrane permeabilization. *Biophys J* 99:3619–3628. <https://doi.org/10.1016/j.bpj.2010.09.027>.
- Lopes SC, Neves CS, Eaton P, Gameiro P. 2012. Improved model systems for bacterial membranes from differing species: the importance of varying composition in PE/PG/cardiolipin ternary mixtures. *Mol Membr Biol* 29:207–217. <https://doi.org/10.3109/09687688.2012.700491>.
- Malanovic N, Lohner K. 2016. Gram-positive bacterial cell envelopes: the impact on the activity of antimicrobial peptides. *Biochim Biophys Acta* 1858:936–946. <https://doi.org/10.1016/j.bbamem.2015.11.004>.
- Malanovic N, Marx L, Blondelle SE, Pabst G, Semeraro EF. 2020. Experimental concepts for linking the biological activities of antimicrobial peptides to their molecular modes of action. *Biochim Biophys Acta Biomembr* 1862:183275. <https://doi.org/10.1016/j.bbamem.2020.183275>.
- Malanovic N, Lohner K. 2016. Antimicrobial peptides targeting gram-positive bacteria. *Pharmaceuticals (Basel)* 9:59. <https://doi.org/10.3390/ph9030059>.

26. Boumann HA, Gubbens J, Koorengel MC, Oh CS, Martin CE, Heck AJ, Patton-Vogt J, Henry SA, de Kruijff B, de Kroon AI. 2006. Depletion of phosphatidylcholine in yeast induces shortening and increased saturation of the lipid acyl chains: evidence for regulation of intrinsic membrane curvature in a eukaryote. *Mol Biol Cell* 17:1006–1017. <https://doi.org/10.1091/mbc.e05-04-0344>.
27. van der Veen JN, Kennelly JP, Wan S, Vance JE, Vance DE, Jacobs RL. 2017. The critical role of phosphatidylcholine and phosphatidylethanolamine metabolism in health and disease. *Biochim Biophys Acta Biomembr* 1859:1558–1572. <https://doi.org/10.1016/j.bbamem.2017.04.006>.
28. den Hertog AL, van Marle J, van Veen HA, Van't Hof W, Bolscher JG, Veerman EC, Nieuw Amerongen AV. 2005. Candidacidal effects of two antimicrobial peptides: histatin 5 causes small membrane defects, but LL-37 causes massive disruption of the cell membrane. *Biochem J* 388:689–695. <https://doi.org/10.1042/BJ20042099>.
29. Fernández-Vidal M, Jayasinghe S, Ladokhin AS, White SH. 2007. Folding amphipathic helices into membranes: amphiphilicity trumps hydrophobicity. *J Mol Biol* 370:459–470. <https://doi.org/10.1016/j.jmb.2007.05.016>.
30. Tossi A, Sandri L, Giangaspero A. 2000. Amphipathic, alpha-helical antimicrobial peptides. *Biopolymers* 55:4–30. [https://doi.org/10.1002/1097-0282\(2000\)55:1%3C4::AID-BIP30%3E3.0.CO;2-M](https://doi.org/10.1002/1097-0282(2000)55:1%3C4::AID-BIP30%3E3.0.CO;2-M).
31. Snider C, Jayasinghe S, Hristova K, White SH. 2009. MPEx: a tool for exploring membrane proteins. *Protein Sci* 18:2624–2628. <https://doi.org/10.1002/pro.256>.
32. Huber A, Hajdu D, Bratschun-Khan D, Gáspári Z, Varbanov M, Philippot S, Fiził A, Czajlik A, Kele Z, Sonderegger C, Galgóczy L, Bodor A, Marx F, Batta G. 2018. New antimicrobial potential and structural properties of PAFB: a cationic, cysteine-rich protein from *Penicillium chrysogenum* Q176. *Sci Rep* 8:1751. <https://doi.org/10.1038/s41598-018-20002-2>.
33. Osumi M. 2012. Visualization of yeast cells by electron microscopy. *J Electron Microscop* (Tokyo) 61:343–365. <https://doi.org/10.1093/jmicro/dfs082>.
34. Manzo G, Ferguson PM, Gustilo VB, Hind CK, Clifford M, Bui TT, Drake AF, Atkinson RA, Sutton JM, Batoni G, Lorenz CD, Phoenix DA, Mason AJ. 2019. Minor sequence modifications in temporin B cause drastic changes in antibacterial potency and selectivity by fundamentally altering membrane activity. *Sci Rep* 9:1385. <https://doi.org/10.1038/s41598-018-37630-3>.
35. Li J, Koh JJ, Liu S, Lakshminarayanan R, Verma CS, Beuerman RW. 2017. Membrane active antimicrobial peptides: translating mechanistic insights to design. *Front Neurosci* 11:73. <https://doi.org/10.3389/fnins.2017.00073>.
36. Shai Y. 2002. Mode of action of membrane active antimicrobial peptides. *Biopolymers* 66:236–248. <https://doi.org/10.1002/bip.10260>.
37. Huang HW, Charron NE. 2017. Understanding membrane-active antimicrobial peptides. *Q Rev Biophys* 50:e10. <https://doi.org/10.1017/S0033583517000087>.
38. Gong Z, Ikononova SP, Karlsson AJ. 2018. Secondary structure of cell-penetrating peptides during interaction with fungal cells. *Protein Sci* 27:702–713. <https://doi.org/10.1002/pro.3364>.
39. Friedrich CL, Moyles D, Beveridge TJ, Hancock RE. 2000. Antibacterial action of structurally diverse cationic peptides on gram-positive bacteria. *Antimicrob Agents Chemother* 44:2086–2092. <https://doi.org/10.1128/AAC.44.8.2086-2092.2000>.
40. Yeaman MR, Yount NY. 2003. Mechanisms of antimicrobial peptide action and resistance. *Pharmacol Rev* 55:27–55. <https://doi.org/10.1124/pr.55.1.2>.
41. Yang Y, Wang C, Gao N, Lyu Y, Zhang L, Zhang S, Wang J, Shan A. 2020. A novel dual-targeted α -helical peptide with potent antifungal activity against fluconazole-resistant *Candida albicans* clinical isolates. *Front Microbiol* 11:548620. <https://doi.org/10.3389/fmicb.2020.548620>.
42. Wong JH, Ng TB, Legowska A, Rolka K, Hui M, Cho CH. 2011. Antifungal action of human cathelicidin fragment (LL13–37) on *Candida albicans*. *Peptides* 32:1996–2002. <https://doi.org/10.1016/j.peptides.2011.08.018>.
43. Ramamourthy G, Park J, Seo C, J Vogel H, Park Y. 2020. Antifungal and antibiofilm activities and the mechanism of action of repeating lysine-tryptophan peptides against *Candida albicans*. *Microorganisms* 8:758. <https://doi.org/10.3390/microorganisms8050758>.
44. Gee ML, Burton M, Grevis-James A, Hossain MA, McArthur S, Palombo EA, Wade JD, Clayton AH. 2013. Imaging the action of antimicrobial peptides on living bacterial cells. *Sci Rep* 3:1557. <https://doi.org/10.1038/srep01557>.
45. Wimley WC. 2015. Determining the effects of membrane-interacting peptides on membrane integrity. *Methods Mol Biol* 1324:89–106. https://doi.org/10.1007/978-1-4939-2806-4_6.
46. Falkenburger BH, Jensen JB, Dickson EJ, Suh BC, Hille B. 2010. Phosphoinositides: lipid regulators of membrane proteins. *J Physiol* 588:3179–3185. <https://doi.org/10.1113/jphysiol.2010.192153>.
47. Clarke OB, Tomasek D, Jorge CD, Dufresne MB, Kim M, Banerjee S, Rajashankar KR, Shapiro L, Hendrickson WA, Santos H, Mancía F. 2015. Structural basis for phosphatidylinositol-phosphate biosynthesis. *Nat Commun* 6:8505. <https://doi.org/10.1038/ncomms9505>.
48. Järvå M, Phan TK, Lay FT, Caria S, Kvensakul M, Hulett MD. 2018. Human β -defensin 2 kills *Candida albicans* through phosphatidylinositol 4,5-bisphosphate-mediated membrane permeabilization. *Sci Adv* 4:eaat0979. <https://doi.org/10.1126/sciadv.aat0979>.
49. Munnik T, Wierchowicka M. 2013. Lipid-binding analysis using a fast blot assay, p 253–260. In Munnik T, Heilmann I (ed), *Plant Lipid Signaling Protocols*. Humana Press, Totowa, NJ.
50. Joshi AS, Zhou J, Gohil VM, Chen S, Greenberg ML. 2009. Cellular functions of cardiolipin in yeast. *Biochim Biophys Acta* 1793:212–218. <https://doi.org/10.1016/j.bbamcr.2008.07.024>.
51. Paradies G, Paradies V, De Benedictis V, Ruggiero FM, Petrosillo G. 2014. Functional role of cardiolipin in mitochondrial bioenergetics. *Biochim Biophys Acta* 1837:408–417. <https://doi.org/10.1016/j.bbabi.2013.10.006>.
52. Kodedová M, Valachovič M, Csáky Z, Sychrová H. 2019. Variations in yeast plasma-membrane lipid composition affect killing activity of three families of insect antifungal peptides. *Cell Microbiol* 21:e13093. <https://doi.org/10.1111/cmi.13093>.
53. Mollinedo F. 2012. Lipid raft involvement in yeast cell growth and death. *Front Oncol* 2:140. <https://doi.org/10.3389/fonc.2012.00140>.
54. Ando J, Kinoshita M, Cui J, Yamakoshi H, Dodo K, Fujita K, Murata M, Sodeoka M. 2015. Sphingomyelin distribution in lipid rafts of artificial monolayer membranes visualized by Raman microscopy. *Proc Natl Acad Sci U S A* 112:4558–4563. <https://doi.org/10.1073/pnas.1418088112>.
55. Bieberich E. 2018. Sphingolipids and lipid rafts: novel concepts and methods of analysis. *Chem Phys Lipids* 216:114–131. <https://doi.org/10.1016/j.chemphyslip.2018.08.003>.
56. Cebecauer M, Amaro M, Jurkiewicz P, Sarmiento MJ, Šachl R, Cwiklik L, Hof M. 2018. Membrane lipid nanodomains. *Chem Rev* 118:11259–11297. <https://doi.org/10.1021/acs.chemrev.8b00322>.
57. Sood R, Kinnunen PK. 2008. Cholesterol, lanosterol, and ergosterol attenuate the membrane association of LL-37(W27F) and temporin L. *Biochim Biophys Acta* 1778:1460–1466. <https://doi.org/10.1016/j.bbamem.2008.02.014>.
58. McHenry AJ, Sciacca MF, Brender JR, Ramamoorthy A. 2012. Does cholesterol suppress the antimicrobial peptide induced disruption of lipid raft containing membranes? *Biochim Biophys Acta* 1818:3019–3024. <https://doi.org/10.1016/j.bbamem.2012.07.021>.
59. Malanovic N, Leber R, Schmuck M, Kriechbaum M, Cordfunke RA, Drijfhout JW, de Breij A, Nibbering PH, Kolb D, Lohner K. 2015. Phospholipid-driven differences determine the action of the synthetic antimicrobial peptide OP-145 on Gram-positive bacterial and mammalian membrane model systems. *Biochim Biophys Acta* 1848:2437–2447. <https://doi.org/10.1016/j.bbamem.2015.07.010>.
60. Sood R, Domanov Y, Pietiäinen M, Kontinen VP, Kinnunen PK. 2008. Binding of LL-37 to model biomembranes: insight into target vs host cell recognition. *Biochim Biophys Acta* 1778:983–996. <https://doi.org/10.1016/j.bbamem.2007.11.016>.
61. Liang Y, Zhang X, Yuan Y, Bao Y, Xiong M. 2020. Role and modulation of the secondary structure of antimicrobial peptides to improve selectivity. *Biomater Sci* 8:6858–6866. <https://doi.org/10.1039/d0bm00801j>.
62. Gelmi ML, D'Andrea LD, Romanelli A. 2020. Application of biophysical techniques to investigate the interaction of antimicrobial peptides with bacterial cells. *Front Med Technol* 2:606079. <https://doi.org/10.3389/fmedt.2020.606079>.
63. Dos Santos Cabrera MP, Rangel M, Ruggiero Neto J, Konno K. 2019. Chemical and biological characteristics of antimicrobial α -helical peptides found in solitary wasp venoms and their interactions with model membranes. *Toxins (Basel)* 11:559. <https://doi.org/10.3390/toxins11100559>.
64. Gopal R, Park JS, Seo CH, Park Y. 2012. Applications of circular dichroism for structural analysis of gelatin and antimicrobial peptides. *Int J Mol Sci* 13:3229–3244. <https://doi.org/10.3390/ijms13033229>.
65. Vida TA, Emr SD. 1995. A new vital stain for visualizing vacuolar membrane dynamics and endocytosis in yeast. *J Cell Biol* 128:779–792. <https://doi.org/10.1083/jcb.128.5.779>.
66. Muñoz A, Marcos JF, Read ND. 2012. Concentration-dependent mechanisms of cell penetration and killing by the de novo designed antifungal hexapeptide PAF26. *Mol Microbiol* 85:89–106. <https://doi.org/10.1111/j.1365-2958.2012.08091.x>.
67. Mochon AB, Liu H. 2008. The antimicrobial peptide histatin-5 causes a spatially restricted disruption on the *Candida albicans* surface, allowing rapid entry of the peptide into the cytoplasm. *PLoS Pathog* 4:e1000190. <https://doi.org/10.1371/journal.ppat.1000190>.

68. Gong Z, Karlsson AJ. 2017. Translocation of cell-penetrating peptides into *Candida* fungal pathogens. *Protein Sci* 26:1714–1725. <https://doi.org/10.1002/pro.3203>.
69. Maniti O, Blanchard E, Trugnan G, Lamazière A, Ayala-Sanmartin J. 2012. Metabolic energy-independent mechanism of internalization for the cell penetrating peptide penetratin. *Int J Biochem Cell Biol* 44:869–875. <https://doi.org/10.1016/j.biocel.2012.02.010>.
70. Veerman EC, Valentijn-Benz M, Nazmi K, Ruissen AL, Walgreen-Weterings E, van Marle J, Doust AB, van't Hof W, Bolscher JG, Amerongen AV. 2007. Energy depletion protects *Candida albicans* against antimicrobial peptides by rigidifying its cell membrane. *J Biol Chem* 282:18831–18841. <https://doi.org/10.1074/jbc.M610555200>.
71. Gyurko C, Lendenmann U, Helmerhorst EJ, Troxler RF, Oppenheim FG. 2001. Killing of *Candida albicans* by histatin 5: cellular uptake and energy requirement. *Antonie Van Leeuwenhoek* 79:297–309. <https://doi.org/10.1023/a:1012070600340>.
72. Chen RC, Lan CY. 2020. Human antimicrobial peptide hepcidin 25-induced apoptosis in *Candida albicans*. *Microorganisms* 8:585. <https://doi.org/10.3390/microorganisms8040585>.
73. Huber A, Galgóczy L, Váradi G, Holzknacht J, Kakar A, Malanovic N, Leber R, Koch J, Keller MA, Batta G, Tóth GK, Marx F. 2020. Two small, cysteine-rich and cationic antifungal proteins from *Penicillium chrysogenum*: a comparative study of PAF and PAFB. *Biochim Biophys Acta Biomembr* 1862:183246. <https://doi.org/10.1016/j.bbmem.2020.183246>.
74. Holzknacht J, Kühbacher A, Papp C, Farkas A, Váradi G, Marcos JF, Manzanares P, Tóth GK, Galgóczy L, Marx F. 2020. The *Penicillium chrysogenum* Q176 antimicrobial protein PAFC effectively inhibits the growth of the opportunistic human pathogen *Candida albicans*. *J Fungi* 6:141. <https://doi.org/10.3390/jof6030141>.
75. Oyinloye BE, Adenowo AF, Kappo AP. 2015. Reactive oxygen species, apoptosis, antimicrobial peptides and human inflammatory diseases. *Pharmaceuticals (Basel)* 8:151–175. <https://doi.org/10.3390/ph8020151>.
76. Silverman JA, Perlmutter NG, Shapiro HM. 2003. Correlation of daptomycin bactericidal activity and membrane depolarization in *Staphylococcus aureus*. *Antimicrob Agents Chemother* 47:2538–2544. <https://doi.org/10.1128/AAC.47.8.2538-2544.2003>.
77. Avitabile C, Moggio L, Malgieri G, Capasso D, Di Gaetano S, Saviano M, Pedone C, Romanelli A. 2012. γ Sulphate PNA (PNA S): highly selective DNA binding molecule showing promising antigene activity. *PLoS One* 7:e35774. <https://doi.org/10.1371/journal.pone.0035774>.
78. Sonderegger C, Galgóczy L, Garrigues S, Fizil Á, Borics A, Manzanares P, Hegedüs N, Huber A, Marcos JF, Batta G, Marx F. 2016. A *Penicillium chrysogenum*-based expression system for the production of small, cysteine-rich antifungal proteins for structural and functional analyses. *Microb Cell Fact* 15:192. <https://doi.org/10.1186/s12934-016-0586-4>.
79. Piller P, Wolinski H, Cordfunke RA, Drijfhout JW, Keller S, Lohner K, Malanovic N. 2022. Membrane activity of LL-37 derived antimicrobial peptides against *Enterococcus hirae*: superiority of SAAP-148 over OP-145. *Biomolecules* 12:523. <https://doi.org/10.3390/biom12040523>.
80. Adell MA, Vogel GF, Pakdel M, Müller M, Lindner H, Hess MW, Teis D. 2014. Coordinated binding of Vps4 to ESCRT-III drives membrane neck constriction during MVB vesicle formation. *J Cell Biol* 205:33–49. <https://doi.org/10.1083/jcb.201310114>.